THE ASTROPHYSICAL JOURNAL, 416:787–805, 1993 October 20

THE MOUNT WILSON OBSERVATORY METALLICITY INDEX, C_{RV}: COMPARISON WITH OTHER PHOTOMETRIC SYSTEMS

W. H. SOON, Q. ZHANG, S. L. BALIUNAS, AND R. L. KURUCZ
Harvard-Smithsonian Center for Astrophysics, 60 Garden Street, Cambridge, MA 02138
Received 1992 December 21; accepted 1993 April 27

ABSTRACT

A new spectrophotometric index, C_{RV}, is assessed as a metallicity indicator for late-type stars. The index is the ratio of the measured photospheric fluxes in 20 Å wide passbands centered at 4001 and 3901 Å. C_{RV} correlates directly with the metallicity index, m_1, of the Strömgren *uvby* system and with the metallicity index *hk*, of Anthony-Twarog et al. (1991).

Using observations of 236 dwarfs and 140 giants combined with stellar atmosphere models (Kurucz 1991), we compared the sensitivity of the C_{RV}, m_1, and *hk* indices to metal abundance. We also studied the sensitivity of the C_{RV}, c_1, and *hk* indices to surface gravity. The effect of interstellar extinction on all the indices was also studied from published mean extinction laws.

We find that the C_{RV} index is sensitive to the variation of metal abundance, [M], over the range examined ($-5.0 \lesssim$ [M] $\lesssim 0.5$). C_{RV} is also more sensitive than the m_1 index at metal-poor conditions ([M] $\lesssim -2.0$). The C_{RV} index has the following advantages: (1) the passbands of C_{RV} are dominated by Fe lines, which reduce the uncertainty that may be introduced by the presence of lines of α-process elements with enhanced abundances at metal-poor conditions; (2) the effect of interstellar reddening is limited because the two passbands are separated in wavelength by only 100 Å. We also find that the atmospheric models produce results that agree qualitatively with the trends of observed indices on stellar parameters such as effective temperature, metallicity, and surface gravity.

Subject headings: stars: abundances — stars: late-type — techniques: spectroscopic

1. INTRODUCTION

The determination of metal abundance is important for the study of solar, stellar, and galactic evolution (see, for example, Eggen, Lynden-Bell, & Sandage 1962; Sandage 1986; Wheeler, Sneden, & Truran 1989; Gilmore, Wyse, & Kuijken 1989). One particularly successful photometric system that provides an effective diagnostic of stellar metal abundance is the Strömgren *uvby* system. The success of the Strömgren *uvby* photometric system has led to the investment of considerable effort in extending the system to metal-poor stars. Recently, Anthony-Twarog et al. (1991, hereafter ATLPT) introduced an additional filter, *Ca*, to the *uvby* system, so that metal abundance can be determined in metal-poor dwarfs and red giants. The *Ca* filter, centered on the Ca II H and K lines (Fig. 1), spans 3800–4100 Å (with 90 Å FWHM) and is used to construct the *hk* index:

$$hk = (Ca - b) - (b - y) . \quad (1)$$

That metallicity index is roughly 3 times more sensitive to metal abundance differences than the m_1 index of the *uvby* system (ATLPT).

Another metallicity indicator that has been quite fruitful in surveying metal-poor stars is based on the *K* indices developed by Beers et al. (1990). We do not study Beers et al.'s indices because synthetic spectra with finer resolution than those used here are required to simulate the *K*6, *K*12, and *K*18 indices (with 6, 12, and 18 Å passbands, respectively).

The idea of using narrow-passband photometry for the determination of stellar properties is not new. Narrow-band photometric indices attempt to combine the best features of both broad-band photometry and high-resolution spectroscopy: they have passbands wide enough to collect enough photons for statistical samplings, yet narrow enough to be sensitive to a wide range of stellar surface conditions. Considering the relative ease in obtaining narrow-band photometric indices and the maturity of models of stellar atmospheres, the potential of such indices as an effective diagnostic of stellar properties is worth closer examination.

One possible metallicity index based on narrow-band fluxes is available from a sustained program of observations of surface magnetic activity in late-type stars made at Mount Wilson Observatory. The HK Project began at the 100 inch (2.5 m) Hooker reflector in 1966 (Wilson 1978), was transferred to the 60 inch (1.5 m) reflector in 1977 (Vaughan, Preston, & Wilson 1978) and expanded to near-nightly observations in 1980 (Baliunas & Vaughan 1985; Baliunas 1991). The studies of surface magnetic activity use the ratio of the chromospheric emission (in 1 Å passbands centered at Ca II H and K lines) to the nearby photospheric fluxes (in two 20 Å passbands centered at 4001 and 3901 Å). The instrument designed for the 60 inch reflector records the photospheric fluxes independently of the chromospheric flux. In principle, the ratio of photospheric fluxes, the C_{RV} index, should yield information on stellar atmosphere properties such as metallicity, surface gravity, or effective temperature.

One goal of this research is the determination of metallicity from the HK Project's data base, which presently contains over 1200 lower–main-sequence and evolved stars. For the approximately 800 lower–main-sequence stars in the sample, metallicity can be compared with age, which can be estimated from the average level of Ca II H and K fluxes (Soderblom, Duncan, & Johnson 1991). In order to evaluate the potential of the C_{RV} index as a metallicity indicator, we will compare it against existing photometric indices and indices computed from theoretical fluxes. We will use the stellar atmosphere

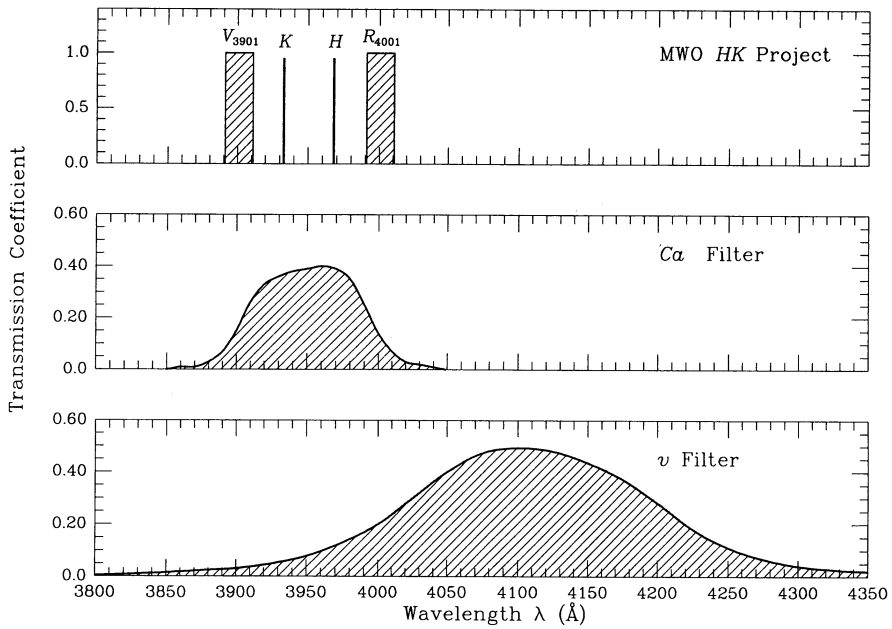

FIG. 1.—R_{4001} and V_{3901} passbands for the C_{RV} index of the Mount Wilson Observatory HK Project, the *Ca* filter introduced by Anthony-Twarog et al. (1991), and the *v* filter of the *uvby* system.

models of Kurucz (1991) to analyze the C_{RV} index in detail and to compare it with the $b-y$ (or preferably a strictly temperature-sensitive index like $V-K$ from the Johnson 11 color photometric system; see, e.g., Cohen, Frogel, & Persson 1978), m_1, and c_1 indices from the *uvby* system and the *hk* index. We will also study the potential effect of reddening on the photometric indices by using two different interstellar mean extinction laws. A more thorough calibration aimed at realizing the full potential of C_{RV} would have to include high-resolution spectroscopy and atmospheric modeling to study specific elemental abundances, e.g., Fe.

2. THE MOUNT WILSON OBSERVATIONS

The program of monitoring stellar activity uses the ratio of the fluxes in the H and K passbands to those of the nearby continuum as an indicator of relative variation of surface magnetic activity, labeled $S \equiv \alpha(N_K + N_H)/(N_V + N_R)$ (see Baliunas 1991). The instrument, the HKP2 spectrophotometer, is described in Vaughan et al. (1978); later modifications of the instrument are discussed in Duncan et al. (1991) and Baliunas et al. (1993). The parameter, α, is a nightly factor determined by measurements of standard stars and a standard lamp in order to maintain the long-term stability of the system. N_K and N_H are the photon counts in the two narrow windows (1 Å wide for dwarfs or 2 Å for giants) centered on the Ca II H and K line cores; N_R and N_V are the counts in the two wider windows (20 Å), labeled as R_{4001} and V_{3901}, centered at 4001 and 3901 Å. Each of the four channels is measured in rapid succession (at a rate of 30 Hz), and the counts in the passbands have been corrected for sky and background illumination. In addition, the position of the channels is translated to compensate for Doppler shifts introduced by the velocity of the star relative to the Earth.

The color index, C_{RV}, introduced by Vaughan et al. (1978), is defined as

$$C_{RV} = 2.5 \log \left(\frac{N_R}{N_V} \right). \quad (2)$$

The index was originally conceived as a temperature-sensitive color index, and has not been discussed in the literature since its introduction. Typical count rates in the R_{4001} and V_{3901} bands are approximately 4500 counts s^{-1} for a G0 V star of magnitude $V = 6.0$. The terrestrial atmospheric transmissions for the R_{4001} and V_{3901} bands differ by about 3% at a zero zenith angle (Hardie 1962). Most observations are made at small zenith distances, making differential atmospheric extinction corrections for one star compared with another for the C_{RV} index negligible.

3. THE DATA

We have focused on the subset of stars in the Mount Wilson HK sample for which Strömgren *uvby* indices are available. For the purposes of this paper, stars are classified in two groups according to their luminosity class: dwarfs (mostly class V, a few VI–V and V–IV) and giants (I, II, III, and IV). Available information on known binary stars is noted in Tables 1 and 2. The components of well-separated binaries (i.e., separation $\gtrsim 3''$) are easily distinguished by our instrument. For a binary system with a smaller separation but large magnitude difference (i.e., $\gtrsim 3$ mag in the blue region of the spectrum) between the program and companion stars, the influence from the companion should be negligible. For those binary systems which have neither a well-resolved separation nor a large magnitude difference (less than 10 stars on our list), the information to disentangle the combined light in the photometric indices is lacking.

Time-averaged indices, $\langle C_{RV} \rangle$, are listed in Tables 1 and 2 for the 236 dwarfs and 140 giants, respectively. The parameter $\sigma_{\langle C_{RV} \rangle}$ gives the standard deviation computed from multiple observations of the stars, and it represents the long-term (interseasonal) variation of the C_{RV} index. If only a single season of observations is available, no value of $\sigma_{\langle C_{RV} \rangle}$ is listed. Note that the intraseasonal variation of the C_{RV} index appears to be large ($\approx$2%–6%; see also Fig. 2), but the variation of the interseasonal average C_{RV} index is generally quite small. The

TABLE 1

DATA FOR DWARFS

HD	$\langle C_{RV} \rangle$	N_{obs}	$\sigma_{\langle C_{RV} \rangle}$	$b-y$	m_1	c_1	$V-K$	Θ_{eff}	log g	[Fe/H]	Double Stars: Δm	Double Stars: Separation (arcsec)	Double Stars: Period
4	0.138	6	...	0.286	0.159	0.689	...	...	...	...	...	...	...
400	0.122	3	...	0.332	0.147	0.386	...	...	...	...	...	...	...
693	0.161	3	...	0.328	0.130	0.405	1.25	0.80	4.1	−0.34	...	...	...
1671	0.088	17	0.015	0.288	0.162	0.566	...	...	...	...	...	...	...
1835	0.247	1562	0.013	0.391	0.216	0.344	...	0.87	4.5	(−0.09, 0.28)	...	...	...
2454	0.089	1416	0.003	0.294	0.138	0.437	...	...	...	...	...	...	...
2913B	0.218	12	...	0.465	0.241	0.277	...	...	...	...	4.0	27.3	...
3229	0.096	1326	0.007	0.303	0.135	0.492	...	...	...	...	...	...	...
3443	0.332	407	0.022	0.427	0.254	0.290	...	0.93	4.6	−0.16	0.0	0.8	25 yr
3651	0.410	1186	0.007	0.509	0.377	0.340	1.89	1.01	4.5	(−0.32, −0.06)	...	...	...
4307	0.153	6	...	0.387	0.185	0.347	...	0.89	3.9	−0.36	...	...	...
4614	0.169	4	0.036	0.372	0.185	0.275	1.47	0.88	4.4	−0.20	3.6	9.7	...
4628	0.458	1184	0.007	0.518	0.415	0.237	2.15	1.02	4.6	−0.29	...	...	...
4813	0.181	3	...	0.334	0.156	0.366	...	0.81	4.5	−0.13	...	...	...
5015	0.146	6	...	0.346	0.193	0.412	1.28	0.84	4.1	0.10	3.0	129.7	...
6301	0.104	6	...	0.294	0.154	0.471	...	...	...	...	...	...	...
6872B	0.130	6	...	0.336	0.155	0.376	...	...	...	...	0.2	14.5	...
6920	0.123	1028	0.007	0.390	0.168	0.410	...	...	...	...	...	...	...
7345	0.143	9	0.004	0.323	0.180	0.435	...	...	...	...	5.7	1.0	9.1 days
7438	0.364	3	...	0.474	0.295	0.273	...	...	...	...	...	...	...
7439	0.142	12	0.031	0.295	0.142	0.442	...	...	...	...	2.2	49.7	...
8799	0.103	12	0.019	0.288	0.148	0.477	...	...	...	...	5.4	134.3	...
9451B	0.346	3	...	0.329	0.201	0.398	...	...	...	...	1.9	17.9	...
9562	0.211	2257	0.006	0.395	0.214	0.389	...	...	...	...	...	...	...
9826	0.143	6	...	0.344	0.179	0.409	1.25	0.83	4.1	−0.14	...	...	...
10307	0.183	6	...	0.389	0.203	0.338	1.39	0.85	4.4	(−0.03, 0.20)	...	...	...
10476	0.391	1059	0.007	0.492	0.364	0.294	2.03	0.97	4.5	−0.20	...	...	...
10700	0.288	1252	0.015	0.445	0.250	0.247	1.82	0.96	4.4	(−0.66, −0.13)	...	...	...
11131	0.211	164	0.014	0.393	0.208	0.293	...	...	...	...	...	...	...
11151	0.112	9	0.018	0.264	0.181	0.505	...	...	...	...	...	...	...
11973B	0.145	24	0.015	0.351	0.199	0.339	...	0.85	4.2	−0.03	1.7	37.4	...
12235	0.193	1116	0.006	0.388	0.208	0.411	...	...	...	...	...	...	...
13421	0.148	2448	0.005	0.358	0.182	0.463	...	...	...	...	...	...	...
13612	0.151	9	0.008	0.358	0.176	0.408	...	...	...	...	0.6	16.2	...
13871	0.108	6	...	0.288	0.171	0.498	...	...	...	...	...	...	...
14082B	0.177	18	...	0.391	0.208	0.293	...	...	...	...	0.4	14.1	...
15524	0.095	6	...	0.269	0.158	0.559	...	...	...	...	4.5	12.9	...
16160	0.534	987	0.010	0.570	0.450	0.350	2.37	...	...	...	...	...	...
16176	0.127	6	...	0.320	0.160	0.463	...	...	...	...	...	...	...
16327	0.116	6	...	0.306	0.170	0.529	...	...	...	...	4.2	21.1	...
16399	0.115	6	...	0.282	0.153	0.513	...	...	...	...	...	...	...
16647	0.119	6	...	0.265	0.157	0.475	...	...	...	...	...	...	...
16673	0.148	1235	0.007	0.331	0.168	0.363	...	0.79	4.3	−0.05	...	...	...
16895	0.106	3	...	0.326	0.165	0.373	1.15	0.84	4.0	(−0.26, 0.07)	5.8	18.2	...
17206	0.164	12	0.016	0.328	0.167	0.406	1.14	...	...	...	...	...	...
17925	0.433	1456	0.010	0.481	0.351	0.295	1.98	0.99	4.6	(−0.15, 0.10)	...	...	...
18256	0.095	1216	0.005	0.308	0.153	0.452	...	...	...	...	...	...	...
18404	0.106	6	...	0.277	0.166	0.483	...	0.76	4.5	0.07	...	...	...
19373	0.156	5	...	0.376	0.201	0.376	1.34	0.86	4.2	0.02	...	...	...
19994	0.165	18	0.027	0.361	0.183	0.424	...	...	...	...	6.4	5.1	...
21794	0.107	6	...	0.343	0.153	0.428	...	...	...	...	3.4	0.1	...
22049	0.443	3625	0.016	0.516	0.419	0.316	2.03	1.00	4.5	−0.20	...	...	17.9 days
22484	0.165	15	0.004	0.368	0.174	0.375	1.34	0.84	4.0	(−0.16, 0.37)	...	...	...
23249	0.424	895	0.035	0.561	0.373	0.385	2.14	1.02	3.8	(−0.27, 0.33)	...	...	...
25329	0.303	2	...	0.528	0.299	0.217	...	1.06	4.5	(−2.30, −1.32)	...	...	...
25457	0.146	24	0.016	0.321	0.168	0.370	...	...	...	...	...	...	...
25570	0.106	2	...	0.249	0.147	0.557	...	...	...	...	...	...	...
25998	0.124	1243	0.005	0.334	0.180	0.373	...	...	...	...	1.7	...	...
26322	0.126	2	...	0.215	0.175	0.752	...	...	...	...	...	...	...
26913	0.235	1165	0.006	0.420	0.245	0.287	...	...	...	...	2.2	65.5	...
26923	0.162	1161	0.008	0.368	0.184	0.331	...	...	...	...	1.0	66.8	...
26965	0.380	799	0.019	0.488	0.322	0.308	2.03	0.99	4.3	(−0.34, 0.01)	5.2	83.5	...
27384	0.306	2	...	0.327	0.113	0.771	...	...	...	...	...	...	...
29140B	0.130	6	...	0.341	0.188	0.347	...	...	...	...	4.0	69.8	3.6 days
29645	0.152	2175	0.005	0.372	0.200	0.397	...	...	...	...	...	...	...
30495	0.233	741	0.022	0.397	0.215	0.316	...	0.84	4.5	0.10	...	...	...
30562	0.226	9	...	0.396	0.209	0.414	...	0.86	3.8	0.13	...	...	...
32147	0.621	678	0.011	0.614	0.601	0.276	...	1.06	4.5	0.02	...	...	SB?
33093	0.186	6	...	0.389	0.184	0.405	...	...	...	...	...	...	...
33256	0.090	9	...	0.300	0.145	0.446	...	0.85	4.1	(−0.60, 0.02)	...	...	...

TABLE 1—*Continued*

HD	$\langle C_{RV} \rangle$	N_{obs}	$\sigma_{\langle C_{RV} \rangle}$	$b-y$	m_1	c_1	$V-K$	Θ_{eff}	log g	[Fe/H]	Double Stars: Δm	Double Stars: Separation (arcsec)	Double Stars: Period
33608	0.140	1027	0.008	0.297	0.176	0.473	...	...	...	...	...	...	...
34411	0.174	12	0.005	0.389	0.206	0.363	1.42	0.88	4.1	(0.06, 0.35)	3.8	146.6	...
35296	0.122	1328	0.006	0.346	0.169	0.349	...	...	...	...	...	...	...
35850	0.170	6	...	0.354	0.182	0.332	...	...	...	...	...	...	...
38382	0.178	6	...	0.359	0.185	0.353	...	...	...	...	...	...	...
39587	0.154	2837	0.007	0.378	0.194	0.307	1.44	0.85	4.5	(−0.12, 0.25)	...	...	...
40832	0.083	6	...	0.290	0.158	0.487	...	...	...	...	...	...	...
43386	0.118	6	...	0.284	0.153	0.438	...	...	...	...	7.0	24.1	...
45067	0.149	2489	0.010	0.359	0.170	0.394	...	...	...	...	...	...	...
48737	0.152	6	...	0.288	0.167	0.052	1.06	...	...	...	...	...	...
50692	0.150	12	0.001	0.376	0.184	0.306	...	...	...	...	...	...	...
51530	0.091	6	0.018	0.348	0.134	0.390	...	...	...	...	...	...	...
52265	0.195	9	0.018	0.358	0.194	0.401	...	...	...	...	...	...	...
55575	0.136	6	...	0.370	0.173	0.294	...	0.86	4.0	(−0.44, −0.21)	...	...	...
58855	0.079	6	...	0.308	0.142	0.390	...	...	...	...	...	...	...
58946	0.113	12	...	0.214	0.155	0.613	0.82	0.70	4.4	−0.31	6.4	213.7	...
61421	0.104	635	0.011	0.272	0.167	0.532	1.01	0.78	4.0	(−0.40, 0.74)	11.2	80.7	40.23 yr
67483	0.088	6	...	0.313	0.152	0.514	...	...	...	...	...	...	...
68146	0.142	9	0.020	0.338	0.148	0.395	...	0.81	...	−0.01	...	...	...
70110	0.180	6	...	0.380	0.194	0.410	...	...	...	...	...	...	...
72905	0.177	698	0.005	0.390	0.206	0.282	...	0.86	4.4	(−0.27, −0.01)	...	...	...
75332	0.123	1767	0.003	0.336	0.184	0.362	...	...	...	...	...	...	...
76151	0.249	1154	0.009	0.412	0.234	0.336	...	0.88	4.5	0.07	...	...	...
76572	0.080	2438	0.003	0.303	0.135	0.504	...	...	...	...	0.0	0.3	...
78366	0.157	1499	0.004	0.377	0.198	0.311	...	...	...	...	...	...	...
81809	0.194	986	0.011	0.418	0.182	0.366	...	0.90	3.8	−0.31	1.0	0.4	...
81997	0.128	3	...	0.296	0.164	0.448	...	...	...	...	...	...	...
82885	0.317	1337	0.010	0.473	0.304	0.372	...	0.92	4.6	0.00	8.5	5.8	...
84737	0.178	9	0.032	0.390	0.203	0.382	1.38	0.86	4.3	−0.04	...	...	...
86728	0.206	3	...	0.416	0.234	0.388	...	0.86	4.3	(−0.11, 0.34)	...	...	...
88355	0.111	728	0.003	0.313	0.151	0.466	...	0.78	...	(−0.10, 0.10)	0.8	0.2	...
88737	0.129	1326	0.005	0.361	0.184	0.440	...	...	...	...	...	...	...
89707	0.175	9	...	0.355	0.140	0.325	...	...	...	...	...	...	...
89744	0.129	2223	0.006	0.336	0.186	0.450	...	...	...	...	...	...	...
90839	0.142	6	...	0.341	0.172	0.331	...	0.83	4.4	−0.23	...	...	...
91889	0.142	21	0.003	0.344	0.149	0.378	...	...	...	...	5.0	14.5	...
92168	0.144	6	0.000	0.368	0.218	0.455	...	...	...	...	...	...	7.8 days
94388	0.168	15	...	0.317	0.174	0.464	...	...	...	...	4.0	134.9	...
95128	0.176	9	0.021	0.392	0.203	0.337	...	0.86	4.3	−0.02	...	...	...
95241	0.113	9	0.014	0.378	0.170	0.376	...	...	...	...	5.6	37.2	...
95735	0.429	1265	0.011	0.979	0.430	0.130	4.16	1.47	4.8	−0.20	...	...	...
97334	0.174	961	0.005	0.392	0.210	0.311	...	...	...	...	...	...	...
97855	0.102	3	...	0.311	0.126	0.410	...	...	...	...	1.3	13.0	...
99491	0.382	3	...	0.482	0.323	0.374	...	0.90	4.6	0.09	1.0	30.5	...
99984	0.089	6	...	0.340	0.148	0.429	...	0.83	3.9	−0.32	...	...	...
100180	0.162	944	0.005	0.367	0.188	0.332	...	...	...	...	2.0	15.9	...
100563	0.135	1533	0.008	0.297	0.172	0.423	...	0.79	4.3	0.12	...	...	...
101198	0.124	6	...	0.338	0.151	0.401	...	...	...	...	5.5	1.7	...
102574	0.182	6	...	0.369	0.197	0.429	...	...	...	...	...	...	...
102870	0.156	18	0.017	0.354	0.187	0.414	1.27	0.83	4.2	(0.10, 0.33)	...	...	...
103095	0.235	1062	0.009	0.484	0.224	0.166	2.07	1.01	4.5	(−1.50, −1.00)	5.5	2.1	...
104304	0.371	5	0.016	0.464	0.304	0.355	...	0.92	4.2	0.18	...	...	...
105421	0.120	6	0.008	0.342	0.143	0.359	...	...	...	...	...	...	...
106516	0.109	1532	0.023	0.319	0.115	0.331	...	0.84	4.5	(−0.98, 0.05)	...	...	853.2 days
107213	0.138	2517	0.006	0.335	0.191	0.453	...	0.80	4.3	0.12	...	...	...
108799	0.183	2	...	0.378	0.188	0.305	...	...	...	...	3.8	1.8	180 yr
108845	0.112	6	...	0.345	0.168	0.415	...	...	...	...	...	...	...
108954	0.152	6	...	0.360	0.181	0.330	...	...	...	...	...	...	...
109358	0.159	15	...	0.385	0.182	0.296	1.43	0.85	4.5	(−0.23, 0.08)	...	...	...
110379	0.090	3	...	0.195	0.168	0.714	0.86	0.72	4.0	(−0.57, −0.07)	0.0	6.6	...
110380	0.122	3	...	0.236	0.160	0.526	...	0.75	4.2	−0.07	0.0	6.6	...
110897	0.127	6	...	0.372	0.153	0.283	1.39	0.88	4.6	−0.30	...	...	...
111456	0.106	529	0.014	0.318	0.156	0.363	...	...	...	...	...	...	...
111998	0.163	3	...	0.313	0.174	0.435	...	...	...	...	...	...	...
113415	0.161	6	...	0.347	0.190	0.379	...	...	...	...	0.5	0.9	...
114174	0.288	3	...	0.422	0.231	0.312	...	...	...	...	...	...	...
114710	0.156	1827	0.008	0.370	0.191	0.337	1.36	0.86	4.5	(0.02, 0.36)	...	...	...
114762	0.108	309	0.002	0.360	0.144	0.285	...	0.88	4.1	(−0.87, −0.59)	...	...	...
115043	0.171	755	0.009	0.388	0.197	0.304	...	0.89	4.3	−0.03	...	...	...
115383	0.171	1069	0.013	0.376	0.191	0.383	...	0.83	4.2	0.04	9.1	34.3	...
115617	0.316	1224	0.035	0.432	0.257	0.320	...	0.90	4.5	−0.02			
117176	0.271	12	0.011	0.446	0.232	0.351	1.74	0.92	3.8	−0.11	...	...	...

TABLE 1—*Continued*

HD	$\langle C_{RV} \rangle$	N_{obs}	$\sigma_{\langle C_{RV} \rangle}$	$b-y$	m_1	c_1	$V-K$	Θ_{eff}	log g	[Fe/H]	Double Stars Δm	Double Stars Separation (arcsec)	Double Stars Period
119124	0.135	3	...	0.346	0.166	0.334	...	...	...	...	3.3	17.9	...
120066	0.211	15	...	0.399	0.189	0.387	...	...	...	...	...	...	...
121560	0.104	6	...	0.335	0.154	0.330	...	...	...	...	...	...	...
122742	0.328	9	...	0.450	0.264	0.318	...	...	...	...	...	...	9.91 yr, SBa
124553	0.242	18	...	0.377	0.188	0.429	...	...	...	...	...	...	...
124570	0.143	3084	0.006	0.343	0.196	0.440	...	0.81	4.2	0.13	...	...	...
124850	0.127	1354	0.012	0.341	0.160	0.449	1.29	0.82	3.8	−0.03	...	...	...
125451	0.104	429	0.008	0.267	0.162	0.484	...	0.76	...	−0.02	...	...	...
126053	0.209	919	0.010	0.402	0.200	0.269	1.57	...	...	...	...	...	...
126660	0.112	9	0.028	0.334	0.156	0.418	...	0.80	4.1	...	...	...	...
128167	0.109	3	...	0.253	0.132	0.488	0.94	0.75	4.4	(−0.50, −0.18)	...	...	
134044	0.131	6	...	0.353	0.165	0.391	...	...	...	...	...	...	...
134083	0.101	463	0.014	0.285	0.165	0.449	1.03	0.76	4.5	0.10	...	...	...
136064	0.185	9	0.024	0.350	0.177	0.422	...	0.84	4.1	−0.03	...	...	...
138268B	0.119	6	...	0.340	0.191	0.368	...	...	...	...	2.3	11.6	...
141004	0.181	1368	0.004	0.385	0.199	0.354	1.39	0.86	4.0	−0.04	...	...	...
142373	0.113	2253	0.007	0.380	0.158	0.322	1.50	0.86	4.3	(−0.45, −0.20)	...	...	...
142860	0.122	12	0.010	0.319	0.151	0.401	1.20	0.81	4.0	(−0.40, −0.07)	...	...	...
142908	0.125	6	0.015	0.233	0.161	0.662	...	...	...	...	...	...	...
143761	0.162	2469	0.009	0.394	0.183	0.322	...	0.87	4.0	−0.17	...	...	...
144284	0.134	3	...	0.354	0.174	0.460	...	0.81	...	0.23	...	...	3.1 days
146233	0.268	33	0.032	0.397	0.221	0.341	...	0.86	4.2	0.02	7.8	25.8	...
147365	0.097	6	0.022	0.268	0.168	0.467	...	...	...	...	5.4	2.0	...
149661	0.407	2609	0.011	0.489	0.352	0.310	1.91	0.94	4.6	0.01	...	...	...
150433	0.205	3	...	0.408	0.204	0.280	...	...	...	...	...	...	...
154345	0.282	6	...	0.446	0.288	0.266	...	...	...	...	...	...	...
154417	0.177	2301	0.005	0.363	0.190	0.327	...	0.87	4.2	−0.19	...	...	...
156026	0.651	1247	0.022	0.667	0.635	0.128	...	1.13	4.7	(−0.34, 0.00)	...	...	...
157241	0.169	21	...	0.409	0.182	0.309	...	0.90	4.3	(−0.58, −0.34)	4.3	230.0	...
157856	0.118	1808	0.004	0.294	0.151	0.495	...	0.81	3.8	−0.17	...	...	...
158614	0.289	1164	0.007	0.437	0.256	0.324	...	0.90	4.4	0.02	0.3	1.4	46.1 yr, SBa
159332	0.106	2944	0.006	0.328	0.148	0.471	...	0.83	3.8	−0.22	...	...	...
160269	0.183	72	0.018	0.383	0.191	0.337	...	...	...	...	4.6	1.7	...
160346	0.542	1783	0.010	0.553	0.506	0.274	...	...	...	...	...	...	...
161239	0.204	1492	0.007	0.420	0.223	0.449	...	...	...	...	...	...	...
162003	0.128	6	...	0.293	0.147	0.497	...	0.77	4.0	0.04	1.2	30.9	...
162004	0.158	6	...	0.343	0.161	0.382	...	0.83	4.2	−0.08	0.8	30.3	...
164259	0.142	9	0.027	0.253	0.154	0.561	...	...	...	...	...	...	...
165401	0.177	6	...	0.414	0.144	0.276	...	...	...	...	...	...	...
166620	0.439	1203	0.008	0.523	0.412	0.332	2.17	1.04	4.5	−0.20	...	...	...
167215	0.098	6	...	0.357	0.148	0.373	...	...	...	...	...	...	...
167216	0.110	6	...	0.346	0.160	0.357	...	...	...	...	...	...	...
168009	0.200	12	...	0.410	0.206	0.340	...	...	...	...	...	...	...
172167	0.207	51	...	0.004	0.156	1.089	0.01	0.54	3.9	(−1.36, 0.20)	9.5	57.1	...
173667	0.112	6	...	0.314	0.150	0.484	...	0.80	4.5	(−0.40, −0.01)	6.7	62.9	...
176095	0.120	1583	0.003	0.310	0.160	0.482	...	0.83	3.7	−0.19	...	...	...
176303	0.113	393	0.008	0.356	0.169	0.452	...	0.82	4.5	−0.05	3.5	18.7	...
176377	0.164	15	...	0.384	0.188	0.286	...	...	...	...	...	...	...
182101	0.113	1571	0.003	0.309	0.137	0.425	...	0.81	4.1	−0.19	...	...	...
184960	0.114	383	0.005	0.320	0.146	0.421	...	0.81	4.5	−0.13	...	...	...
185144	0.367	1031	0.009	0.472	0.320	0.261	1.91	0.98	4.4	−0.25	...	...	...
185395	0.099	3	...	0.261	0.158	0.506	...	0.77	4.4	(−0.21, 0.10)	6.0	48.4	...
186408	0.213	116	0.027	0.410	0.214	0.375	1.43	0.86	4.3	(0.00, 0.22)	0.2	39.0	...
186427	0.221	111	0.016	0.416	0.226	0.354	1.55	0.87	4.4	0.00	0.2	39.0	...
186760	0.184	6	...	0.381	0.182	0.427	...	...	...	...	...	...	...
187013	0.100	2728	0.007	0.316	0.155	0.435	...	0.82	4.0	(−0.35, 0.10)	3.3	25.9	...
187691	0.162	2781	0.003	0.356	0.188	0.404	...	0.82	4.4	0.14	8.5	22.9	...
188512	0.332	971	0.004	0.521	0.306	0.341	2.02	0.98	3.8	(−0.23, 0.29)	7.9	12.5	...
189340	0.203	14	0.023	0.371	0.194	0.328	...	...	...	...	...	...	...
190007	0.614	1422	0.009	0.658	0.654	0.176	...	...	...	...	...	...	...
190406	0.188	1683	0.004	0.389	0.197	0.321	...	...	...	...	...	...	...
194012	0.124	1683	0.003	0.338	0.162	0.342	...	...	...	...	...	...	...
195838	0.189	6	...	0.350	0.167	0.417	...	...	...	...	...	...	...
196310B	0.159	18	0.042	0.356	0.171	0.331	...	...	...	...	...	...	...
197373	0.118	8	0.014	0.302	0.140	0.459	...	0.78	4.5	−0.03	...	...	...
199960	0.246	6	...	0.406	0.209	0.397	...	...	...	...	...	...	...
200790	0.184	6	...	0.346	0.171	0.423	...	0.82	4.5	−0.05	...	...	...
201091	0.578	2137	0.009	0.656	0.677	0.134	2.83	1.17	4.5	−0.06	0.7	24.9	...
201092	0.474	2168	0.008	0.791	0.676	0.067	3.30	1.30	4.6	(−0.65, 0.00)	0.7	24.9	...
203454	0.128	6	...	0.352	0.173	0.326	...	0.82	4.5	−0.13	...	...	3.2 days
205626	0.114	3	...	0.365	0.164	0.444	...	...	...	...	...	...	...
205627	0.105	3	...	0.356	0.174	0.399	...	...	...	...	...	...	...

TABLE 1—*Continued*

HD	$\langle C_{RV}\rangle$	N_{obs}	$\sigma_{\langle C_{RV}\rangle}$	$b-y$	m_1	c_1	$V-K$	Θ_{eff}	log g	[Fe/H]	Double Stars: Δm	Double Stars: Separation (arcsec)	Double Stars: Period
206826	0.094	12	0.044	0.314	0.154	0.404	1.18	0.82	4.3	−0.22	1.4	6.6	...
206860	0.163	2191	0.011	0.379	0.190	0.305	...	...	...	...	...	...	...
207958	0.126	9	0.015	0.247	0.153	0.541	...	...	...	...	...	...	...
207978	0.071	2842	0.005	0.309	0.108	0.439	...	0.82	4.0	−0.59	...	...	...
210277	0.341	6	...	0.459	0.298	0.353	...	...	...	...	...	...	...
212697	0.325	3	...	0.391	0.216	0.271	...	0.88	...	0.30	0.3	10.0	...
212754	0.135	2540	0.004	0.332	0.178	0.433	...	0.82	4.5	−0.04	6.5	3.0	...
213429	0.202	9	0.011	0.356	0.188	0.342	...	...	...	...	...	...	...
215648	0.107	9	0.011	0.330	0.147	0.407	...	0.86	4.1	(−0.28, −0.05)	8.0	12.2	...
216385	0.106	2435	0.003	0.320	0.149	0.433	...	0.83	4.0	(−0.62, −0.33)	...	...	...
217014	0.232	1253	0.006	0.416	0.232	0.364	1.51	0.88	4.3	0.12	...	...	...
217926	0.115	63	0.006	0.271	0.146	0.623	...	...	...	...	...	...	...
218261	0.192	6	...	0.350	0.185	0.363	...	0.82	4.5	0.09	...	...	...
219487	0.115	3	...	0.276	0.146	0.468	...	...	...	...	...	...	...
219623	0.159	9	0.059	0.352	0.171	0.396	...	0.83	4.1	−0.10	...	...	...
220117	0.108	6	...	0.296	0.170	0.489	...	0.78	4.5	−0.05	...	...	...
222368	0.139	12	0.010	0.329	0.164	0.395	...	0.83	4.0	(−0.51, 0.09)	...	...	...
223346	0.126	3	...	0.304	0.136	0.471	...	...	...	...	...	...	SB?
223421	0.099	6	...	0.277	0.140	0.546	...	...	...	...	...	...	...
223552	0.117	9	...	0.258	0.148	0.472	...	...	...	...	...	21.6	...
224635	0.099	3	...	0.347	0.176	0.348	...	0.83	4.9	−0.07	0.0	3.8	...
224930	0.177	1338	0.007	0.428	0.189	0.215	1.81	0.97	4.4	(−1.08, −0.52)	2.7	66.8	26.27 yr

NOTE.—The averaged $\langle C_{RV}\rangle$ index and related statistics (N_{obs} = number of observed points; $\sigma_{\langle C_{RV}\rangle}$ = standard deviation of observed points) for the sample of dwarfs. The quantities $b-y$, m_1, and c_1 are the observed indices of the *uvby* system adopted for this work. $V-K$ is the observed index from the Johnson 11 color photometric system. Θ_{eff} ($=5040\ K/T_{eff}$), log g, and [Fe/H] are the observed stellar effective temperature, surface gravity, and scaled iron abundance, respectively. The characteristics of the binary system associated with the program stars are taken from the third edition of the Bright Star Catalogue (Hoffleit 1964) and the Eighth Catalogue of the Orbital Elements of Spectroscopic Binary Systems (Batten, Fletcher, & MacCarthy 1989). We also searched (via SIMBAD) for recent indications of duplicity from spectroscopic or speckle observations. (Δm, Separation, Period) are the magnitude difference, maximum observed separation, and, if known, orbital period of the two components (or two brightest components) of a visual binary (or a multiple system), respectively. The symbols SBa and SB? identify the primary star to be associated with a known or suspected spectroscopic binary system.

relatively large intraseasonal variation of the C_{RV} index is due to an early decision in the creation of the current Mount Wilson *HK* data base in 1977 to store the values of C_{RV} directly in a logarithmic form which does not retain the full precision of the data. We are in the process of recovering the full precision of C_{RV} from the original records in the archive.

The values of the $b-y$, m_1, c_1, and $V-K$ indices are taken from the compilation in the SIMBAD data base. The photometric indices adopted here are as they were presented; therefore, the interstellar reddening corrections to those indices for some of the distant field giants may need to be addressed [e.g., the metal-poor giants HD 195636 and BD −18°5550 in Table 2 have measured reddening values $E(B-V)$ of 0.06 and 0.12, respectively; Bond 1980; Peterson & Carney 1989]. For most of the dwarfs, the interstellar reddening corrections for all the indices are assumed to be small, since they are within 25 pc of the Sun.

Stellar properties such as Θ_{eff} ($= 5040\ K/T_{eff}$), log g, and [Fe/H] are also listed in Tables 1 and 2. [Fe/H] denotes the scaled solar abundance and is defined as log $(Fe/H)_*$ − log $(Fe/H)_\odot$, where the asterisk and Sun symbol denote stellar and solar-related properties, respectively. The purpose of listing those parameters is to allow us to interpolate from the grid of photometric indices computed from the model atmospheres. The primary source of the stellar atmosphere data is the collection of Cayrel de Strobel et al. (1992), which is based mostly on available results from high-dispersion spectra. When the determinations of [Fe/H] from different sources differ by more than 0.2 dex, the ranges of the [Fe/H] values are presented.

The longevity of the HK Project allows us to investigate the question of long-term variability of the C_{RV} index. The records of the index for several stars over roughly the past 10 years are shown in Figure 2. Knowledge of the time dependence of C_{RV} is important because of an index which purports to represent a macroscopic property such as metallicity should not be associated with a large-amplitude time-dependent phenomenon. This caveat arises because of the increasing popularity of the selection of filters which contain the Ca II H or K emission features, e.g., the *hk* index of ATLPT and the *K* index of Beers et al. (1990). The extent of variability of Ca II H and K emission features which may be caused by long-term stellar magnetic activity variability is largely unknown in metal-deficient and evolved stars. For example, compare the Ca II H and K flux records of two low-metallicity stars (Fig. 3): HD 103095 shows cyclic variability, while HD 122563 is relatively inactive. Twarog & Anthony-Twarog (1991) have reported the variation of the *hk* index in one of the metal-poor stars, CD −38°245, by about 20% in an interval of 2.5 years, which could indicate magnetic activity variability over long time scales. Thus further study of surface magnetic activity and its variability should be an adjunct in interpreting the indices including the Ca II H and K fluxes.

4. THEORETICAL CALCULATIONS OF THE *uvby*, C_{RV}, AND *hk* PHOTOMETRIC INDICES

Kurucz's (1991) grid of model atmospheres was used to compute all the photometric indices studied here. The theoretical treatment of opacity in the grid includes over 58 million atomic and molecular lines. The model of the solar atmosphere reproduces the observed solar energy distribution quite well. With the increased refinement of the opacity data, the com-

TABLE 2

DATA FOR GIANTS

HD	$\langle C_{RV} \rangle$	N_{obs}	$\sigma_{\langle C_{RV} \rangle}$	$b-y$	m_1	c_1	$V-K$	Θ_{eff}	log g	[Fe/H]	Double Stars: Δm	Double Stars: Separation (arcsec)	Double Stars: Period
3421	0.195	141	0.010	0.540	0.310	0.390	...	...	...	...	...	...	...
4744	0.391	3	...	0.652	0.288	0.464	...	...	...	...	...	...	...
6186	0.323	42	0.010	0.580	0.360	0.400	2.28	...	...	...	...	...	...
6210	0.123	12	0.005	0.356	0.183	0.475	...	...	...	...	...	...	...
6903	0.137	1182	0.006	0.435	0.189	0.484	...	...	...	...	...	...	...
7218	0.114	33	...	0.292	0.162	0.456	...	...	...	...	...	...	...
9270	0.304	48	0.011	0.605	0.374	0.393	2.19	...	...	...	7.0	1.4	...
9927	0.592	2	...	0.765	0.653	0.402	2.78	1.12	1.7	−0.03	...	...	...
12929	0.462	72	0.013	0.696	0.526	0.395	2.63	1.11	1.4	(−0.29, −0.08)	...	...	...
12953	−0.100	148	0.010	0.488	−0.066	0.643	1.74	...	...	...	...	...	...
13174	0.141	60	0.008	0.210	0.185	0.874	...	...	...	...	...	...	...
13611	0.235	45	0.010	0.540	0.330	0.440	2.06	...	...	...	...	...	...
14489	−0.108	25	0.020	0.321	−0.038	0.753	...	...	...	...	6.8	11.7	...
16246B	0.114	118	0.020	0.266	0.169	0.477	...	...	...	...	0.6	38.6	1.1 days
17484	0.105	88	0.008	0.269	0.180	0.678	...	...	...	...	...	...	SB?
17506	0.566	2	...	1.100	0.670	0.350	3.70	1.17	1.0	−0.15	4.5	28.6	...
18925	0.252	2	...	0.442	0.214	0.694	1.95	...	...	...	7.7	57.7	14.66 yr
20894	0.302	2	...	0.547	0.317	0.417	...	...	...	...	...	...	...
21120	0.247	346	0.006	0.547	0.335	0.424	2.02	...	...	...	...	...	4.53 yr
22211	0.130	272	0.007	0.408	0.183	0.448	...	...	...	...	...	...	...
23230	0.111	1	...	0.267	0.184	0.977	1.17	...	...	...	8.0	31.4	...
27022	0.224	370	0.007	0.510	0.289	0.405	1.86	...	...	...	...	...	...
28271	0.102	58	0.005	0.346	0.171	0.493	...	...	...	...	2.0	15.4	...
28307	0.325	619	0.004	0.580	0.390	0.389	2.10	...	...	...	...	...	...
29139	0.608	159	0.007	0.955	0.814	0.373	3.67	1.29	1.2	(−0.33, 0.00)	10.2	121.7	...
30606	0.164	12	...	0.345	0.181	0.456	...	...	...	...	...	...	...
31398	0.587	268	0.011	0.937	0.775	0.307	3.32	...	...	0.00	...	...	...
31964	−0.006	133	0.030	0.426	0.016	1.286	1.53	...	...	...	6.3	207.7	27.10 yr
35984	0.087	137	0.007	0.308	0.150	0.532	...	...	...	...	...	...	...
36389[a]	0.555	41	0.017	1.440	0.480	0.650	5.23	1.36	0.7	0.11	...	...	...
36994	0.087	133	0.014	0.288	0.161	0.557	...	...	...	...	...	...	...
39364	0.370	41	0.038	0.621	0.289	0.441	2.54	1.10	2.5	−0.50	...	...	...
43905	0.115	80	0.010	0.284	0.171	0.632	...	...	...	...	...	...	6.5 days
47205	0.533	137	0.026	0.625	0.522	0.389	2.32	1.02	3.1	0.07	...	...	...
48329	0.452	316	0.015	0.869	0.654	0.283	2.76	1.10	0.8	−0.05	6.0	111.6	...
50037	0.114	12	...	0.331	0.161	0.461	...	...	...	...	...	...	...
50778	0.644	35	0.017	0.871	0.716	0.436	3.42	1.27	1.9	−0.03	...	...	...
57006	0.118	12	...	0.338	0.169	0.472	...	...	...	...	...	...	...
61064	0.121	640	0.011	0.289	0.169	0.653	...	0.79	3.2	0.44	7.3	26.0	...
62345	0.300	44	0.019	0.573	0.379	0.398	2.11	1.22	...	(−0.20, 0.00)	4.5	6.8	...
62509	0.371	128	0.007	0.611	0.427	0.420	2.25	1.05	2.6	(−0.51, 0.16)	7.7	201.1	...
66011	0.150	18	0.001	0.360	0.193	0.474	...	...	...	...	...	...	...
67228	0.182	340	0.008	0.406	0.207	0.402	...	0.86	4.2	0.05	...	...	...
67594	0.259	42	0.042	0.597	0.361	0.445	2.04	...	...	...	3.5	67.1	...
69267	0.623	90	0.007	0.911	0.765	0.367	3.41	1.17	1.9	−0.21	10.5	29.2	...
71369	0.218	417	0.010	0.522	0.308	0.422	1.92	0.97	2.3	−0.02	7.0	177.2	...
72779	0.136	1520	0.003	0.441	0.206	0.466	...	...	...	...	...	...	...
73598	0.330	531	0.004	0.591	0.400	0.377	2.19	...	...	...	...	...	...
73665	0.339	523	0.004	0.603	0.407	0.455	2.16	...	...	...	...	...	...
73710	0.370	502	0.008	0.626	0.435	0.405	2.25	...	...	...	0.5	63.4	...
73974	0.330	476	0.006	0.603	0.400	0.411	2.13	...	...	...	...	...	...
74739	0.305	47	0.011	0.608	0.403	0.407	2.14	1.04	2.0	0.20	2.1	30.7	...
82210	0.231	455	0.010	0.488	0.254	0.347	1.89	0.95	3.6	−0.38	...	...	...
82328	0.079	166	0.014	0.314	0.153	0.463	1.16	0.80	3.9	(−0.20, 0.01)	10.7	5.1	...
82635	0.278	320	0.010	0.562	0.346	0.389	...	...	...	...	...	...	...
83273	0.131	386	0.006	0.357	0.188	0.460	...	...	...	...	...	...	...
84441	0.184	44	0.013	0.509	0.275	0.456	1.83	0.93	2.4	−0.13	...	...	...
89025	0.127	222	0.022	0.196	0.169	0.986	0.82	...	...	...	...	...	...
89449	0.106	113	0.018	0.297	0.171	0.459	1.15	0.97	...	−0.02	...	...	...
95272	0.486	45	0.036	0.662	0.468	0.420	2.45	1.05	3.0	0.10	...	...	...
95689	0.376	62	...	0.660	0.437	0.394	2.44	1.08	2.2	−0.19	9.1	0.9	44 yr, SBa
96833	0.450	54	0.017	0.703	0.524	0.396	2.57	1.11	1.7	(−0.39, −0.07)	...	...	...
97561	0.260	207	0.008	0.457	0.250	0.383	...	...	...	...	...	...	...
98262	0.576	50	0.014	0.880	0.690	0.360	3.18	1.24	2.1	−0.19	6.4	7.4	...
99028	0.118	273	0.033	0.267	0.172	0.606	...	0.76	4.0	0.08	3.2	3.2	192 yr, SBa
99904	0.112	546	0.021	0.326	0.181	0.482	...	...	...	...	...	...	...
111199	0.141	122	0.020	0.351	0.168	0.489	...	...	...	...	6.2	16.5	...
111812	0.119	315	0.007	0.435	0.193	0.411	1.56	...	...	...	...	...	...
114642	0.131	120	0.037	0.313	0.147	0.473	...	0.78	4.0	−0.15	...	...	...
120933	0.503	74	0.013	1.090	0.620	0.650	4.61	...	...	...	...	...	...
121370	0.150	309	0.017	0.376	0.203	0.476	1.31	0.90	3.8	(0.16, 0.44)	...	...	495 days

TABLE 2—*Continued*

HD	$\langle C_{RV} \rangle$	N_{obs}	$\sigma_{\langle C_{RV} \rangle}$	$b-y$	m_1	c_1	$V-K$	Θ_{eff}	log g	[Fe/H]	Double Stars: Δm	Double Stars: Separation (arcsec)	Double Stars: Period
122563	0.079	599	0.018	0.633	0.090	0.550	2.53	1.10	1.2	(−3.00, −2.35)	...	...	...
124897	0.476	862	0.013	0.755	0.526	0.491	3.07	1.15	1.7	(−0.81, −0.30)	...	...	...
127539	0.089	121	0.014	0.298	0.146	0.518	...	...	...	...	...	...	...
134792	0.087	48	0.013	0.287	0.157	0.461	...	...	...	...	...	...	...
135722	0.315	51	0.019	0.587	0.346	0.410	2.27	1.05	2.7	−0.50	4.2	105.4	...
137510	0.187	12	...	0.397	0.214	0.441	...	...	...	...	...	...	...
137759	0.537	18	0.021	0.711	0.567	0.429	2.61	...	...	...	...	...	...
138525	0.120	12	...	0.348	0.164	0.448	...	...	...	...	...	...	...
140573	0.547	54	0.025	0.715	0.572	0.445	2.57	1.10	2.0	(−0.07, 0.37)	9.0	61.5	...
142357	0.103	78	0.010	0.279	0.152	0.648	...	...	...	...	6.4	3.5	SB?
143107	0.520	57	0.018	0.751	0.570	0.414	2.85	...	...	...	8.4	2.2	...
144608	0.268	252	0.024	0.521	0.283	0.448	2.00	...	...	...	...	...	...
148317	0.167	63	0.012	0.414	0.195	0.438	...	...	...	...	...	...	...
150680	0.171	117	0.012	0.415	0.207	0.408	1.51	1.02	...	0.26	3.5	1.7	34.4 yr
151769	0.127	156	0.033	0.307	0.161	0.536	...	...	...	...	...	...	...
156697	0.168	71	0.007	0.250	0.158	0.904	...	...	...	...	...	...	...
157482	0.184	526	0.012	0.442	0.205	0.460	...	...	...	...	...	...	SB?
159026	0.113	75	0.010	0.327	0.192	0.773	...	...	...	...	...	...	...
159181	0.212	493	0.010	0.610	0.323	0.423	2.01	0.94	1.4	(0.10, 0.30)	9.7	115.6	...
160365	0.112	189	0.014	0.382	0.151	0.573	...	...	...	...	...	...	SB?
161096	0.554	44	0.022	0.721	0.549	0.453	2.55	1.09	2.4	0.14	...	...	...
161149	0.153	71	0.018	0.273	0.168	0.798	...	...	...	...	...	...	...
161797	0.268	115	0.013	0.464	0.279	0.413	1.65	0.97	4.1	(0.10, 0.48)	6.7	33.7	...
163770	0.498	524	0.009	0.830	0.660	0.320	2.84	...	...	...	...	...	...
164058	0.634	18	0.011	0.943	0.811	0.374	3.56	1.22	1.6	(−0.23, 0.33)	8.8	125.4	...
164136	0.104	78	0.010	0.254	0.141	0.901	1.18	0.74	3.4	−0.26	...	...	...
167944	0.294	385	0.016	0.469	0.174	0.718	...	...	...	...	...	...	...
173399	0.279	511	0.011	0.550	0.285	0.354	...	...	...	...	0.1	25.8	...
178449	0.119	66	0.011	0.253	0.144	0.708	...	...	...	...	3.3	128.1	42.9 days
182900	0.118	200	0.008	0.302	0.169	0.541	...	...	...	...	...	...	...
182901	0.113	161	0.011	0.282	0.168	0.511	...	...	...	...	...	...	...
185758	0.165	59	0.032	0.497	0.260	0.466	1.73	...	...	...	8.8	33.0	...
185958	0.342	66	0.017	0.630	0.450	0.410	2.24	...	...	...	...	...	...
186155	0.133	208	0.010	0.264	0.203	0.718	...	...	...	...	...	...	...
186791	0.597	395	0.018	0.936	0.760	0.294	3.31	...	...	0.00	...	...	...
190390	0.110	12	...	0.424	0.170	1.033	...	...	...	...	...	...	...
192455	0.173	12	...	0.334	0.186	0.464	...	0.82	3.8	0.00	...	...	...
192876	0.318	51	0.034	0.571	0.327	0.389	2.34	...	...	...	5.0	45.5	...
195636	−0.005	13	...	0.466	0.028	0.386	...	0.92	3.4	−2.79	...	...	...
197101	0.135	65	0.008	0.223	0.186	0.806	...	...	...	...	...	...	...
197989	0.374	51	0.006	0.627	0.415	0.425	2.35	1.06	2.8	(−0.25, 0.08)	9.0	44.3	SB?
198149	0.350	219	0.009	0.553	0.366	0.375	2.15	1.06	3.0	(−0.50, 0.23)	7.7	100.5	...
198809	0.233	441	0.010	0.510	0.310	0.390	...	...	...	...	...	...	SB?
200723A	0.127	63	0.010	0.242	0.183	0.760	...	...	...	...	2.0	57.0	...
201507	0.151	63	0.023	0.242	0.168	0.668	...	...	...	...	...	...	...
202109	0.309	138	0.012	0.591	0.446	0.296	2.11	1.02	2.0	0.10	...	...	...
203504	0.459	45	0.010	0.654	0.516	0.424	2.45	...	...	...	4.1	36.3	3.04 yr
203842	0.129	305	0.008	0.304	0.178	0.619	...	...	...	...	...	...	...
204075	0.272	44	0.023	0.603	0.416	0.116	1.88	0.97	1.6	−0.15	10.0	21.5	6.30 yr
204867	0.202	577	0.022	0.513	0.326	0.554	1.77	0.92	1.3	(−0.05, 0.20)	7.9	35.7	...
205435	0.260	289	0.015	0.540	0.330	0.370	2.05	0.89	2.0	−0.18	...	...	...
206453	0.307	298	0.015	0.540	0.310	0.410	...	...	...	...	...	...	...
206778	0.537	290	0.016	0.964	0.681	0.300	3.20	1.21	1.0	(−0.25, −0.02)	6.0	144.7	...
206859	0.321	42	0.019	0.709	0.468	0.354	2.42	1.04	1.2	−0.03	...	...	...
208110	0.161	78	0.000	0.514	0.188	0.423	...	...	...	...	...	...	...
209166	0.125	439	0.007	0.238	0.152	0.739	...	...	...	...	5.4	54.7	...
209750	0.245	466	0.012	0.598	0.380	0.437	1.97	0.96	1.4	(0.03, 0.31)	...	...	...
210459	0.110	69	0.012	0.304	0.177	0.778	...	...	...	...	...	...	...
210460	0.180	414	0.005	0.462	0.199	0.334	...	...	...	...	...	...	...
210807	0.286	240	0.006	0.560	0.360	0.380	...	...	...	...	...	...	...
215182A	0.262	30	0.016	0.535	0.296	0.499	2.02	...	...	...	7.1	91.0	818 days
216397	0.629	51	0.018	1.000	0.750	0.450	...	...	...	...	7.0	29.6	...
219291	0.069	365	0.007	0.310	0.137	0.543	...	...	...	...	...	...	...
219576	0.533	39	0.016	1.190	0.210	1.050	...	...	...	...	...	...	...
219734	0.539	21	0.011	1.090	0.660	0.510	4.49	...	...	...	8.0	7.7	...
220657	0.123	78	0.011	0.390	0.186	0.461	1.39	...	...	...	...	...	...
222399	0.115	33	...	0.228	0.178	0.736	...	...	...	...	3.4	14.9	...
222404	0.482	28	0.029	0.616	0.498	0.407	...	1.04	2.8	(−0.05, 0.27)	...	...	...
BD −18°5550	0.073	32	...	0.690	−0.045	0.400	2.71	1.10	1.0	(−3.00, −2.70)	...	...	...
CD −38°245	...	...	...	0.590	0.048	0.428	2.33	1.06	1.5	(−4.50, −3.00)	...	...	...

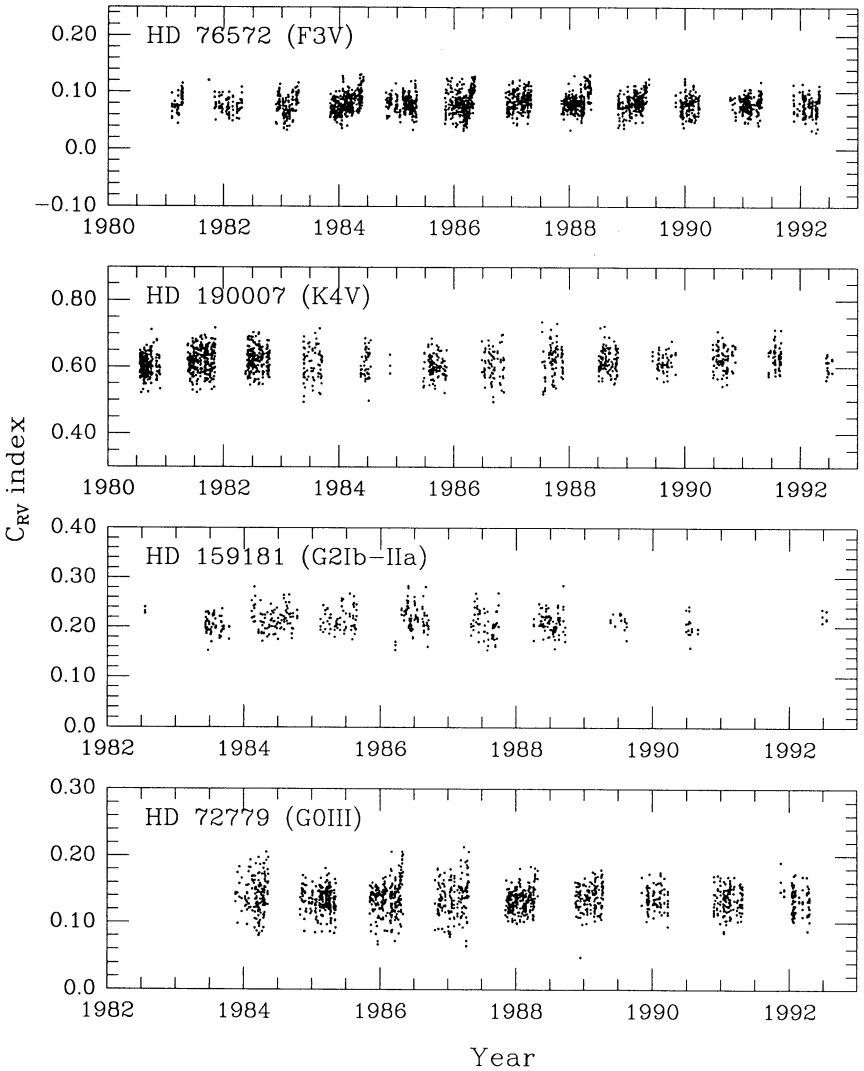

FIG. 2.—Examples of time series of the C_{RV} index for two dwarfs (HD 75672 and HD 190007) and two giants (HD 159181 and HD 72779). Note that the seasonal spread of the data is primarily caused by rounding error in the data base and is not related to rotation modulation produced by surface inhomogeneities.

puted fluxes would seem to have credibility for a differential analysis of the broad-band and intermediate-band photometry.

The analysis presented rests on a grid of atmospheric models computed in the following ranges:

$$3500\ \mathrm{K} \leq T_{\mathrm{eff}} \leq 10{,}000\ \mathrm{K}\ , \tag{3}$$

$$0.0 \leq \log g \leq 5.0\ , \tag{4}$$

$$V_{\mathrm{turb}} = 2\ \mathrm{km\ s^{-1}}\ , \tag{5}$$

$$[M] = [-5.0], [-4.5], [-4.0], [-3.5], [-3.0], [-2.5], [-2.0], [-1.5], [-1.0], [-0.5], [-0.3], [-0.2], [-0.1], [0.0], [+0.1], [+0.2], [+0.3], [+0.5]\ . \tag{6}$$

Examples of the synthetic flux distributions are shown in Figure 4.

Despite recent progress made on the models, their possible shortcomings should also be noted so that the reliability of our

NOTES TO TABLE 2

NOTE.—The averaged $\langle C_{RV} \rangle$ index and related statistics (N_{obs} = number of observed points; $\sigma_{\langle C_{RV} \rangle}$ = standard deviation of observed points) for the sample of giants. The quantities $b - y$, m_1, and c_1 are the observed indices of the *uvby* system adopted for this work. $V - K$ is the observed index from the Johnson 11 color photometric system. Θ_{eff} ($= 5040\ \mathrm{K}/T_{\mathrm{eff}}$), log g, and [Fe/H] are the observed stellar effective temperature, surface gravity, and scaled iron abundance, respectively. The characteristics of the binary system associated with the program stars are taken from the third edition of the Bright Star Catalogue (Hoffleit & Jaschek 1964) and the Eighth Catalogue of the Orbital Elements of Spectroscopic Binary Systems (Batten et al. 1989). We also searched (via SIMBAD) for recent indications of duplicity from spectroscopic or speckle observations. (Δm, Separation, Period) are the magnitude difference, maximum observed separation, and, if known, orbital period of the two components (or two brightest components) of a visual binary (or a multiple system), respectively. The symbols SBa and SB? identify the primary star to be associated with a known or suspected spectroscopic binary system.

[a] Note that the reddest giant on the list HD 36389 has $b - y = 1.440$ and is not plotted in all the $(b - y)$-dependent plots.

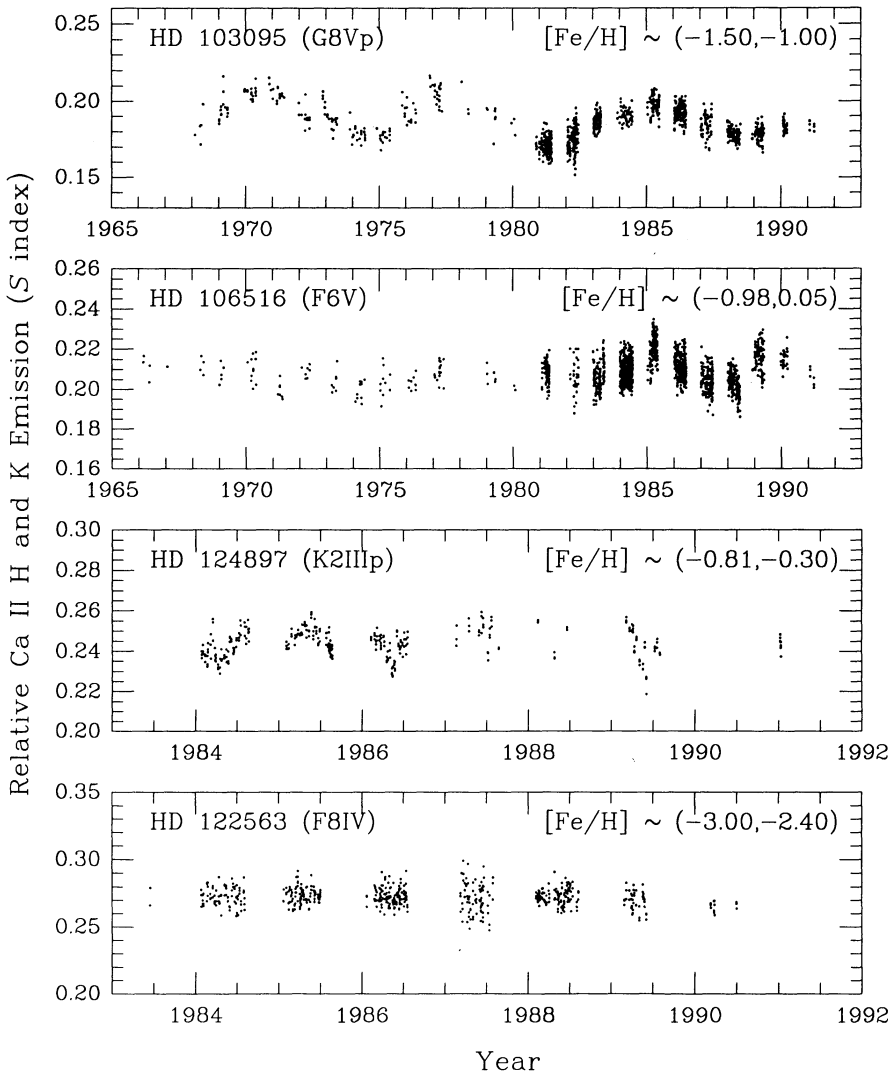

FIG. 3.—Examples of surface magnetic activity (characterized by relative Ca II H and K emission fluxes—the S index) for some of the metal-deficient stars (two dwarfs measured with 1 Å wide Ca II H and K passbands: HD 103095 and HD 106516, and two giants observed with 2 Å wide H and K passbands: HD 124897 and HD 122563).

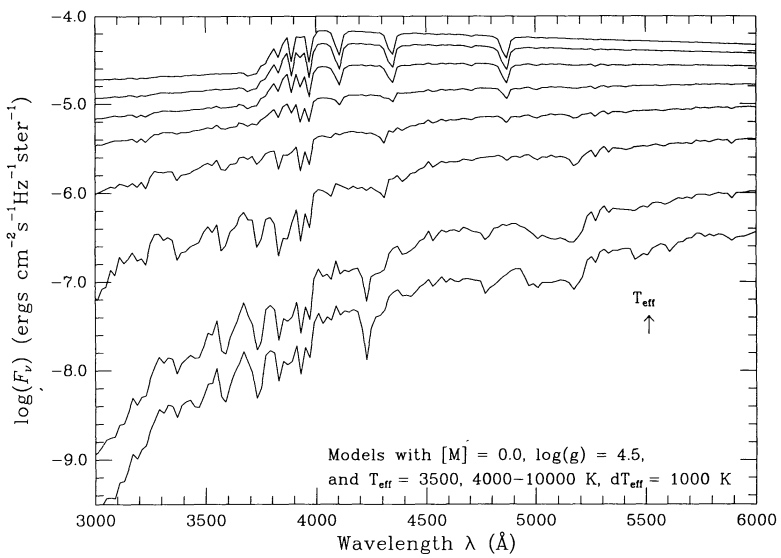

FIG. 4.—Examples of synthetic spectra used in the computation of all the photometric indices discussed in this work. The stellar atmosphere models shown are for $[M] = 0.0$, $\log g = 4.5$, and $T_{\rm eff} = 3500$, 4000, 5000, 6000, 7000, 8000, 9000, and 10,000 K. The arrow indicates the direction of increasing $T_{\rm eff}$ for the models.

results can be assessed. First, we must limit application of the grid to effective temperatures above 3500 K because opacity data for triatomic molecules which become important at cool temperatures are lacking. Second, the models may not be applicable to the low-gravity cases where non-LTE effects dominate. Third, the abundance of the heavy elements is scaled with respect to the solar abundances of Anders & Grevesse (1989). Therefore, the possible enhancement of the light metal elements such as Mg, Si, Ca, and Ti due to the α-process, particularly for the metal-poor stars, is not considered in the construction of the grid.

Since calculation of the *uvby* colors has been discussed by Relyea & Kurucz (1978), the details of the procedure will not be reiterated. To calibrate the theoretical *uvby* colors, we first identified the model from the improved grid of models (Kurucz 1991) that best reproduces both the spectrophotometry and the Balmer line profiles of Vega, and then forced the computed colors to match the observed colors. The recent abundance analysis of Vega by Adelman & Gulliver (1990) indicates that Vega is slightly metal-poor. Therefore, we adopted the model atmosphere with $T_{\rm eff} = 9400$ K, $\log g = 3.90$, and [M] $= -0.5$ for Vega.

We also computed values of C_{RV} from the theoretical fluxes. In accordance with the calibration of the *uvby* indices, we also used Vega to calibrate the computed C_{RV} index. However, we note that the resolution of the theoretical flux is only 20 Å. Thus, the computed C_{RV} index is based just on the average of the two nearest flux points. Synthetic spectra will be computed by Kurucz in the future with finer spectral resolution that will allow more accurate integration.

Similarly, we computed theoretical values of the *hk* index of ATLPT over the full range of the grid. To calibrate the theoretical *hk* index to the measured values, we forced the computed *hk* indices (adopting the model with $T_{\rm eff} = 9250$ K, $\log g = 4.0$, and [M] $= 0.0$) to match the measured *hk* index for the standard star HD 83373 (A1 V). That star was chosen because it has closest spectral type classification to that of Vega, which was not observed by ATLPT.

5. EFFECTS OF INTERSTELLAR EXTINCTION

As noted, most of the dwarfs on our list are nearby stars, and the effect of reddening on the photometric indices should be small. However, the photometric indices for some of the more distant giants (e.g., HD 195636 and BD $-18°5550$) should be noticeably reddened. In Figure 5 we examine the effects of

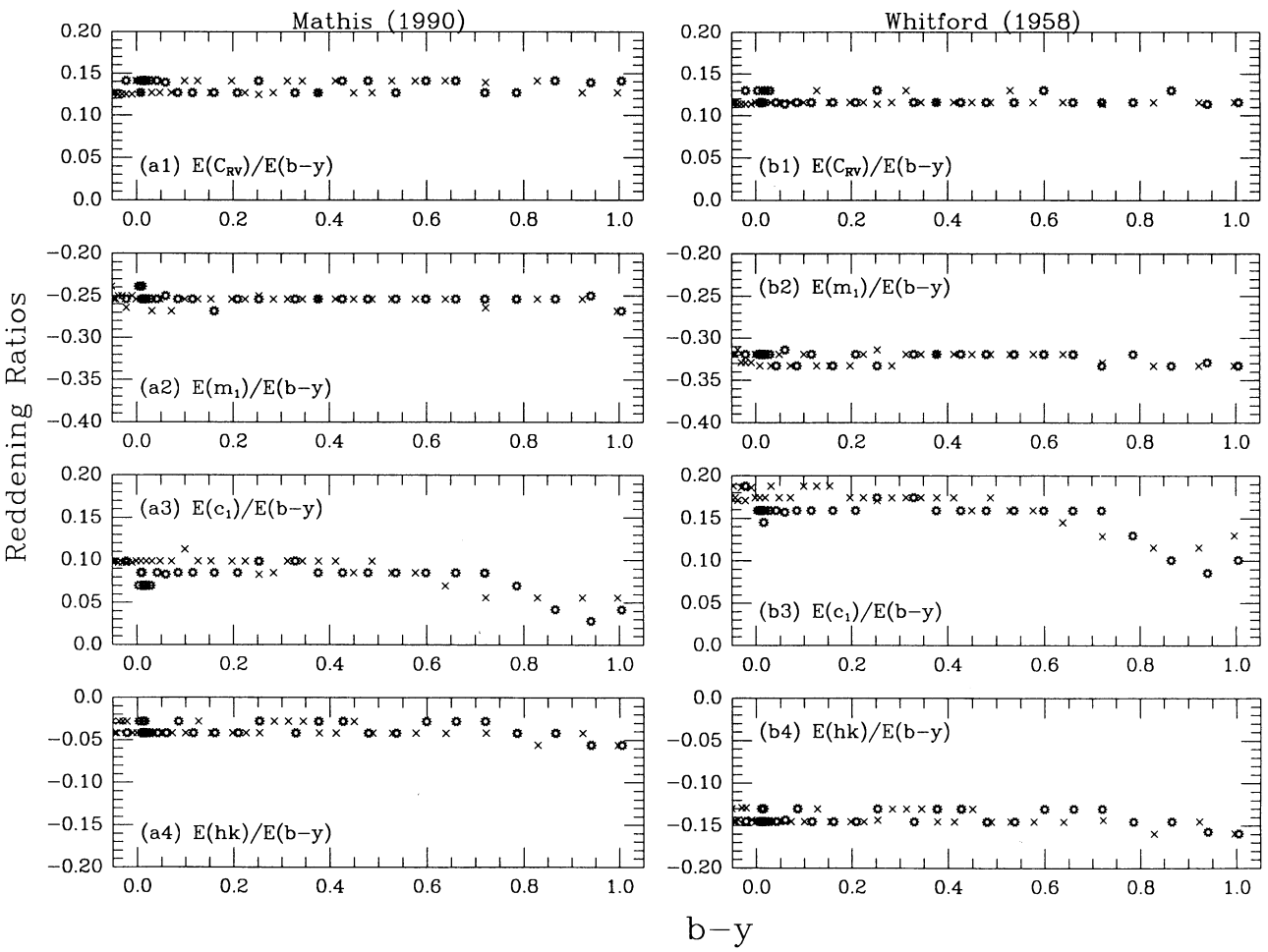

FIG. 5.—Reddening ratios $E(C_{RV})/E(b-y)$, $E(m_1)/E(b-y)$, $E(c_1)/E(b-y)$, and $E(hk)/E(b-y)$ computed by applying the mean extinction law from Mathis (1990) (*left*) and Whitford (1958) (*right*) to the synthetic spectra of Kurucz (1991). Values of the optical total-to-selective extinction ratio, $R_V = 3.1$ (for the diffuse interstellar medium), and $E(B-V) = 0.1$ were adopted. Crosses denote the $\log g = 4.5$, [M] $= 0.0$ grid points, while open symbols denote the $\log g = 2.0$, [M] $= 0.0$ grid points.

interstellar extinction on all the photometric indices using the "mean extinction laws" proposed by Mathis (1990) and Whitford (1958). We assumed a value of the optical total-to-selective extinction ratio, $R_V[\equiv A(V)/E(B-V)] = 3.1$, for the diffuse dust in the interstellar medium, where $A(V)$ is the absolute visual extinction and $E(B-V) = 0.1$. We convolved the synthetic fluxes of Kurucz (1991) (for the [M] = 0.0 grid) with the two proposed extinction laws and calculated all the reddening ratios by subtracting the reddened indices from the non-reddened indices.

In all cases considered, the computed reddening ratios are only weak functions of $T_{\rm eff}$ and log g, except for the c_1 index at low temperatures. The averages of the computed reddening ratio $E(b-y)/E(B-V)$ are 0.71 and 0.69 for the extinction law of Mathis (1990) and Whitford (1958), respectively. However, the computed reddening ratios for the m_1, c_1, and hk indices depend strongly on the chosen extinction law. For the C_{RV} index, the reddening ratio is less sensitive to the extinction law applied because its passbands are only 100 Å apart. The averages of the reddening ratios, $E(m_1)/E(b-y) \approx -0.32$ and $E(hk)/E(b-y) \approx -0.14$, calculated using the extinction law of Whitford (1958), are close to the values estimated by ATLPT. However, the mean value of $E(hk)/E(b-y) \approx -0.04$ calculated by applying the extinction law of Mathis (1990) is significantly smaller than the estimate of -0.155 quoted by ATLPT. A comparison of the C_{RV}, m_1, and hk indices indicates that the C_{RV} and hk indices are substantially less impacted by reddening owing to the close proximity and the symmetric arrangement of the filter passbands involved.

6. DISCUSSION

The average values of the observed index, $\langle C_{RV}\rangle$, for the 236 dwarfs (*crosses*) and 140 giants (*open symbols*) are plotted as a function of $b-y$ in Figures 6*a* and 6*b*, respectively. Theoretical grids with log $g = 4.5$ are used to represent the dwarfs, while grids with log $g = 2.0$ are adopted for the giants. The corresponding plots of m_1 versus $b-y$ for these stars are shown in Figures 7*a* and 7*b*. In addition, the observed hk versus $b-y$ relations for the dwarfs and giants from Table 4 of ATLPT are plotted with theoretical grids in Figures 8*a* and *b*.

In Figure 9 we show the dependence of the $\langle C_{RV}\rangle$ index on [M] or log g in terms of the $V-K$ index for a smaller subset of the stars shown previously in Figures 6*a* and 6*b*. The $V-K$ indices were calculated and calibrated to Vega according to the

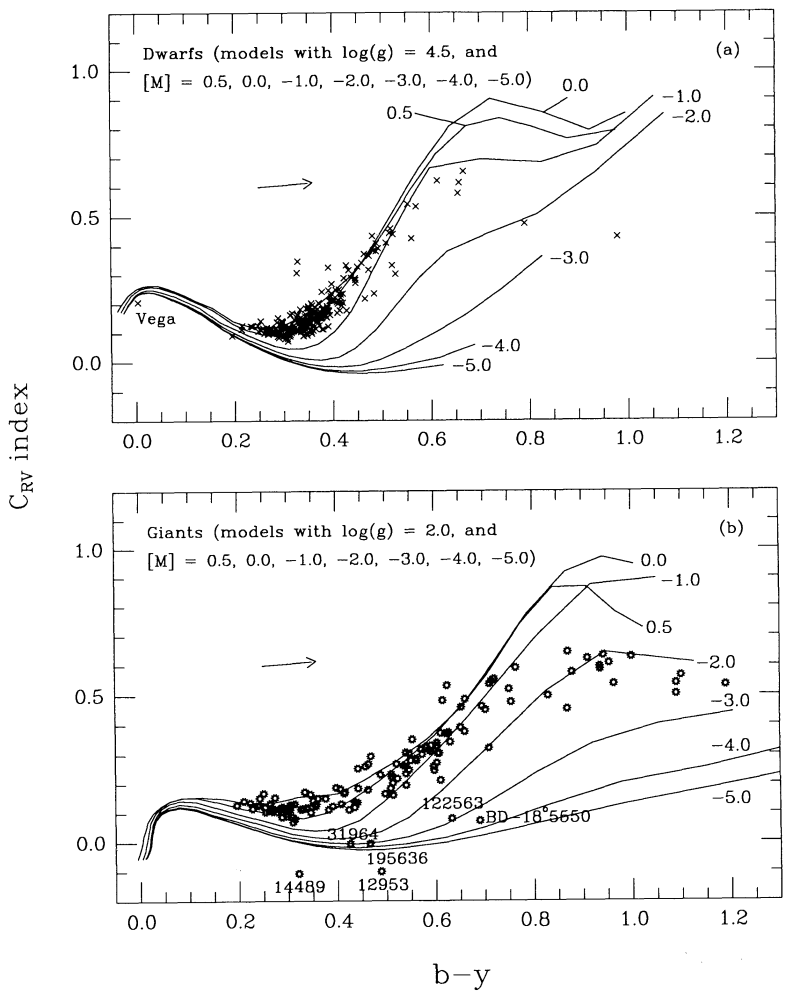

FIG. 6.—$\langle C_{RV}\rangle$ vs. $b-y$ indices observed for the sample of (*a*) dwarfs (*crosses*) and (*b*) giants (*open symbols*) in the HK Project. The grids are computed from atmosphere models with [M] = 0.5, 0.0, −1.0, −2.0, −3.0, −4.0, −5.0, and log $g = 4.5$ and 2.0 for typical dwarfs and giants, respectively. The arrows in (*a*) and (*b*) indicate the effect of interstellar reddening computed with $E(b-y) = 0.10$ [assuming the mean value $E(C_{RV})/E(b-y) \approx 0.13$ from the results of the Mathis 1990 extinction law; see Fig. 5]. Metal-poor giants of particular interest are labeled (see text).

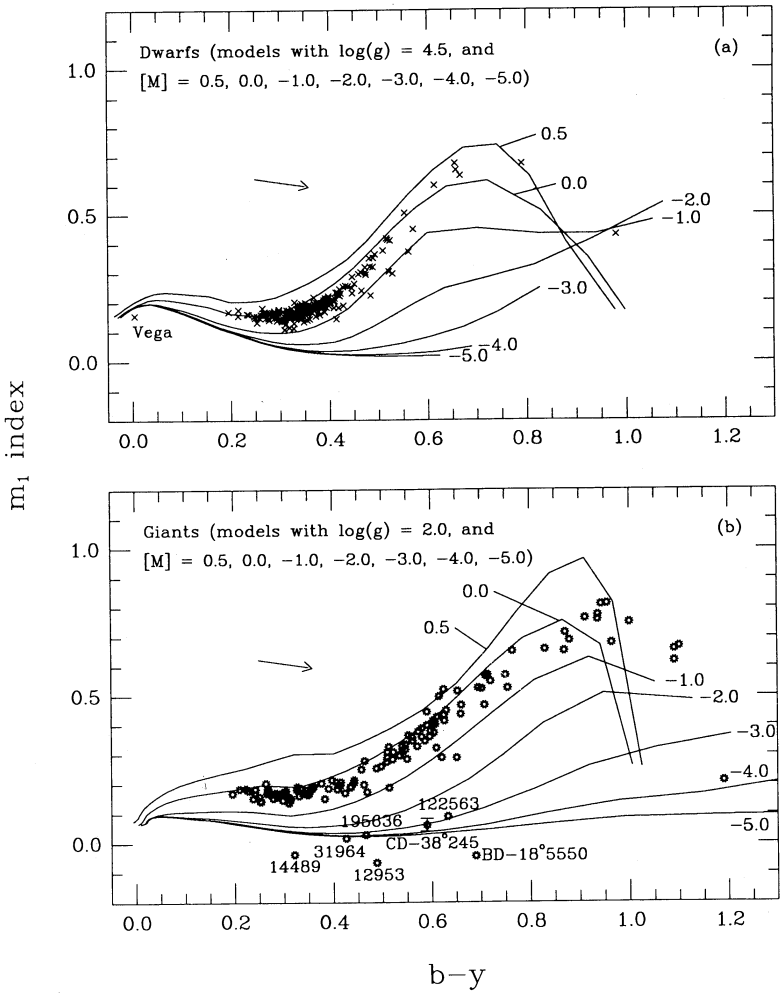

FIG. 7

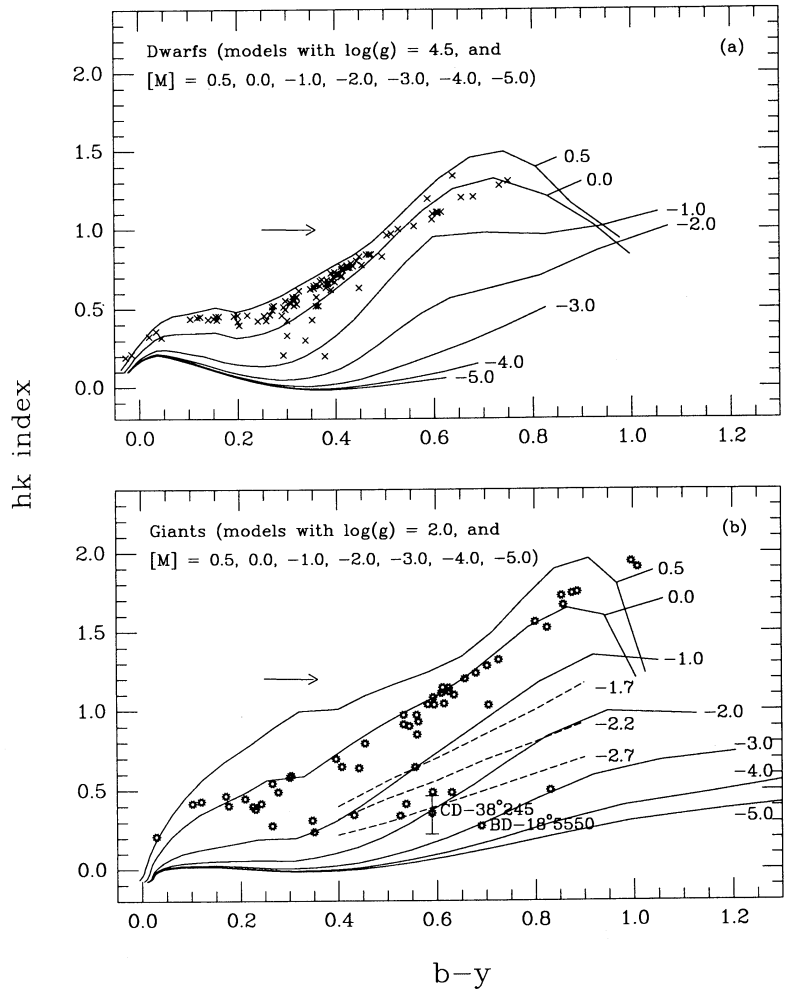

FIG. 8

FIG. 7.—Observed m_1 vs. $b - y$ indices for the sample of (*a*) dwarfs (*crosses*) and (*b*) giants (*open symbols*) studied by the HK Project. The grids are computed from atmosphere models with [M] = 0.5, 0.0, −1.0, −2.0, −3.0, −4.0, −5.0, and log g = 4.5 and 2.0 for typical dwarfs and giants, respectively. The arrows in (*a*) and (*b*) indicate the effect of interstellar reddening computed with $E(b - y) = 0.10$ [assuming the mean value $E(m_1)/E(b - y) \approx -0.25$ from the results of the Mathis 1990 extinction law; see Fig. 5]. Metal-poor giants of particular interest are labeled (see text). The full range of the time variability of the m_1 index noted by Twarog & Anthony-Twarog (1991) in the star CD −38°245 is shown by the vertical bar.

FIG. 8.—Observed *hk* vs. $b - y$ indices for the sample of (*a*) dwarfs (*crosses*) and (*b*) giants (*open symbols*) from Table 4 of Anthony-Twarog et al. (1991). The grids (*solid lines*) are computed from atmosphere models with [M] = 0.5, 0.0, −1.0, −2.0, −3.0, −4.0, −5.0, and log g = 4.5 and 2.0 for typical dwarfs and giants, respectively. The arrows in (*a*) and (*b*) indicate the effect of interstellar reddening computed with $E(b - y) = 0.10$ [assuming the mean value $E(hk)/E(b - y) \approx -0.04$ from the results of the Mathis 1990 extinction law; see Fig. 5]. The full range of the time variability of the *hk* index noted by Twarog & Anthony-Twarog (1991) in the star CD −38°245 is shown by the vertical bar. Note that Twarog & Anthony-Twarog's (1991) isometallicity curves (*dashed lines*) of the *hk* index for [Fe/H] = −1.7, −2.2, and −2.7 are different from ours (see text).

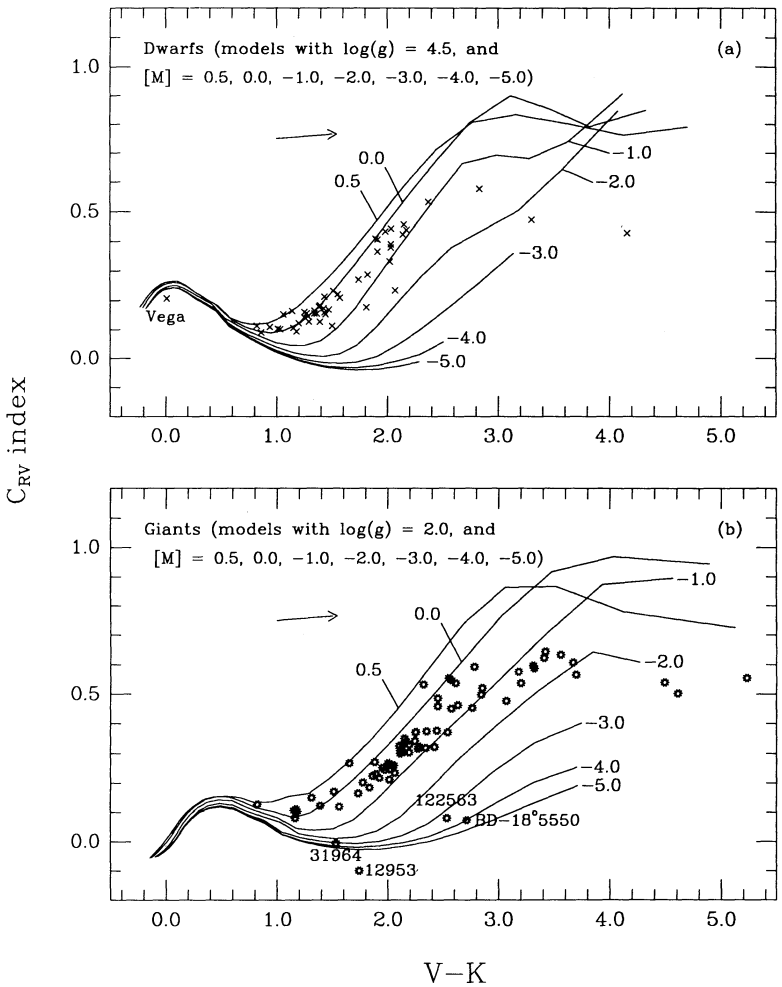

FIG. 9.—$\langle C_{RV}\rangle$ vs. $V-K$ indices observed for a subset of the sample of (*a*) dwarfs (*crosses*) and (*b*) giants (*open symbols*) from the HK Project (see Figs. 6*a* and 6*b*, respectively). The arrows in (*a*) and (*b*) indicate the effect of interstellar reddening assuming $E(V-K) = 0.50$ and

$$\frac{E(C_{RV})}{E(V-K)} = \left[\frac{E(C_{RV})}{E(b-y)}\right]\left[\frac{E(b-y)}{E(B-V)}\right]\left[\frac{E(B-V)}{E(V-K)}\right] \approx (0.13)(0.7)\left(\frac{1}{2.78}\right) \approx 0.033.$$

We note that the computed $E(V-K)/E(B-V)$ ratio show a slight dependence on $T_{\rm eff}$ (not shown here), and we had adopted the averaged $E(V-K)/E(B-V)$ of 2.78. The grids are computed from atmosphere models with [M] = 0.5, 0.0, −1.0, −2.0, −3.0, −4.0, −5.0, and log g = 4.5 and 2.0 for typical dwarfs and giants, respectively.

procedure described in § 4. Compared with C_{RV} versus $b-y$ (Figs. 6*a* and 6*b*), the use of $V-K$ makes C_{RV} sensitive to metallicity, even for $0.5 \lesssim$ [M] $\lesssim -1.0$, an interval previously obscured in the $[C_{RV}, (b-y)]$-plane. That lack of sensitivity to metallicity is caused by the slight dependence of $b-y$ on [M] or log g. The $V-K$ index has a dependence on effective temperature that is better defined than for the $b-y$ or $B-V$ indices. Moreover, the $b-y$ and $B-V$ indices are also sensitive to abundance and surface gravity. The confusion caused by $b-y$ in the determination of [M] or log g is particularly noticeable for a narrow passband index like C_{RV}, but is less significant for larger passband indices such as m_1, c_1, and *hk*. We conclude that $V-K$ is better suited to studying the sensitivity of the narrow passband index C_{RV} on abundance or surface gravity.

The qualitative behavior of the calculated C_{RV}, m_1, and *hk* indices agrees well with the observed trends. For example, the *hk* index in ATLPT's list over the entire range of spectral type (A–K) is narrowly confined for the dwarfs and widely spaced in the giants (i.e., the range of log g is narrower for dwarfs). Those observed features of the *hk* index are well reproduced by the computed grids. Such predictability affirms that the approach of using model atmospheres in the search of better photometric indices is meaningful.

We have also included in Figure 8*b* the isometallicity calibration curves of ATLPT for metal-poor red giants with [Fe/H] = −1.7, −2.2, −2.7. The differential sense of their calibration curves for low metallicity agrees with the computed grids. However, the absolute scale of the computed and calibrated isometallicity curves is significantly offset. Although no certain resolution of the disagreement of the absolute scales can be offered, we suggest that the Ca abundance may be enhanced due to the α-process in metal-poor conditions (e.g., Wheeler et al. 1989). In that case, the current comparisons may

be inappropriate and may require that models with enhanced α-process elements be used in computing the *hk* grid for [M] $\lesssim -1.0$.

6.1. *Sensitivity of the C_{RV} Index to Properties of Stellar Atmospheres*

Examination of the solar spectrum in the wavelength region in and near the R_{4001} and V_{3901} passbands of C_{RV} reveals that line blanketing is dominated by Fe I and Fe II absorption lines. Other metallic features, such as the absorption lines of Sc, Ti, V, Mn, and Co, are present but relatively rare. The Ca lines, which are included in other photometric indices but not in C_{RV}, are subject to α-process enhancement in metal-poor stars (e.g., Wheeler et al. 1989). As noted, the variability of the chromospheric Ca II H and K lines is relatively unexplored in late-type giants and metal-poor stars, and such variability could affect the determination of metallicity. In spite of the relatively larger passbands involved in other photometric indices, it is important to note that the contribution of the Ca II H and K emission features to the flux in the passband can be significant at low-metallicity conditions because the H and K lines become more prominent compared with the weakened atomic (ionic) lines and molecular bands of the background photospheric radiation. In turn, such photometric indices would become more sensitive to the variability in the Ca II H and K emission features at low metallicity conditions than at solar abundances. The absence of the Ca atomic and ionic lines in the C_{RV} passbands avoids these possible complications. The dominance of Fe lines in C_{RV} also allows for a less ambiguous correlation with iron abundance compared with the broad-band photometric indices.

A summary of the sensitivity of C_{RV} to effective temperature (C_{RV} versus $b-y$ and $V-K$), scaled abundance [M] (C_{RV} versus m_1 and *hk*), and surface gravity (C_{RV} versus c_1 and *hk*) follows.

6.1.1. *Temperature Dependence*

A comparison of the temperature sensitivity of the C_{RV} index to $b-y$ or $V-K$ shows that C_{RV} correlates well with the wider passband indices in the temperature range 4000 K $\lesssim T_{\rm eff} \lesssim$ 8000 K. As expected, with C_{RV}'s narrower passbands and shorter wavelengths, it does not have any particular advantage compared with the Strömgren or Johnson indices in temperature sensitivity. In fact, the disadvantage of C_{RV} is that the fluxes are smaller in the narrower passbands, which makes observations less time-efficient.

6.1.2. *Abundance Dependence*

As noted, the choice of a suitable parameter is critical in deciphering the sensitivity of the C_{RV} index on [M]. Figures 9*a* and 9*b* show that the C_{RV} index has a well-defined and systematic dependence on [M] over the entire range $-5.0 \lesssim$ [M] $\lesssim 0.5$. On the other hand, if the [M]-dependence of the C_{RV} index were to be studied with the $b-y$ index (Figs. 6*a* and 6*b*), then the trend becomes indeterminate at values between the solar and intermediate abundance ($-1.0 \lesssim$ [M] $\lesssim 0.5$). That comparison reveals the weak dependence of the $b-y$ index on abundance and surface gravity. It also calls for the $V-K$ index in the study of the [M] or log *g* sensitivity of the C_{RV} index. At present, observations of the $V-K$ index are less readily available than the $b-y$ index for our sample of stars.

At low metallicity, the C_{RV} index seems to perform better than the m_1 index (compare Figs. 6*b* and 7*b*). Particularly, we note that the observed values of C_{RV} for the three known metal-poor giants on our list (HD 122563, HD 195636, BD $-18°5550$) agree well with the computed indices. On the other hand, the observed values of the traditional metallicity index, m_1, do not seem to fit the computed grid at low values of [M]. There are two A-type supergiants on our list, HD 12953 (A1 Iae) and HD 14489 (A2 Iab), that seem to be out of the range of our grids of computed C_{RV} index. No explanation readily accounts for that discrepancy. However, one possibility is that those stars may have an enhanced helium abundance, as has been observed in some anomalous A-type supergiants in the Magellanic Clouds (Humphreys, Kudritzki, & Groth 1991). The computed grids would be inappropriate for stars with an enhanced helium abundance.

The study of the dependence of C_{RV} on [M] has several important and direct implications for the determination of the net chromospheric emission, $R'_{\rm HK}$ (Noyes et al. 1984), from the measured Ca II H and K activity index, *S*. The parameter $R'_{\rm HK}$ provides a measure of the level of stellar surface magnetic activity that is suitable for studying the magnetic activity–age relationship (Soderblom et al. 1991). The results of our analysis justify the use of the adopted temperature-dependent correction of the photospheric flux for stars in Noyes et al. (1984), since the range of [M] covered by the sample is mostly within $-0.5 \lesssim$ [M] $\lesssim 0.5$. However, our analysis calls for both temperature- and metallicity-dependent correction factors for the derivation of $R'_{\rm HK}$ in metal-poor stars. This is because, at metal-poor conditions, the photospheric fluxes of the continuum passbands at 4001 and 3901 Å are significantly elevated compared with the fluxes at solar abundance.

6.1.3. *Surface Gravity Dependence*

The general trends in Figures 6*a* and 6*b* seem to suggest that the C_{RV} index is also sensitive to surface gravity. Such behavior is verified in Figure 10*a*, where the C_{RV} was shown to be weakly dependent on log *g*. As stated previously, the $b-y$ index may be sensitive to log *g*; therefore, it is preferable to determine the log *g* dependence of all the indices from the $V-K$ index. The available measurements of c_1 versus $V-K$ for the stars on our list are plotted in Figure 10*b*. In addition, we have studied the sensitivity of the *hk* index to log *g* in Figure 10*c*. The *hk* index has a roughly linear dependence on surface gravity at low log *g* ($\lesssim$2.0), but as log *g* increases further, the gravity dependence of this index becomes complex. The dwarf and giant branches are more clearly separated by the c_1 index than by *hk* and C_{RV}, particularly at high temperatures (i.e., $0.0 \lesssim V-K \lesssim 2.0$).

6.2. *Comparisons between Measured and Calculated Photometric Indices*

The direct comparisons of the observed and calculated C_{RV}, $b-y$, m_1, c_1, and *hk* indices for all the stars with available stellar atmosphere parameters ($\Theta_{\rm eff}$, log *g*, [Fe/H]) are given in Figures 11–15. For stars with a range of [Fe/H] values listed in Tables 1 and 2, we adopt the median value of [Fe/H] to determine the theoretical indices from the computed grids.

The difference of each index is plotted as a function of measured $T_{\rm eff}$, log *g*, and [Fe/H]. In general, the differences of the indices are larger for cooler stars. This is likely due to the increasing uncertainty of the atmospheric models at low temperatures. The difference of the indices also seems to be weakly dependent on surface gravity (i.e., differences are larger for

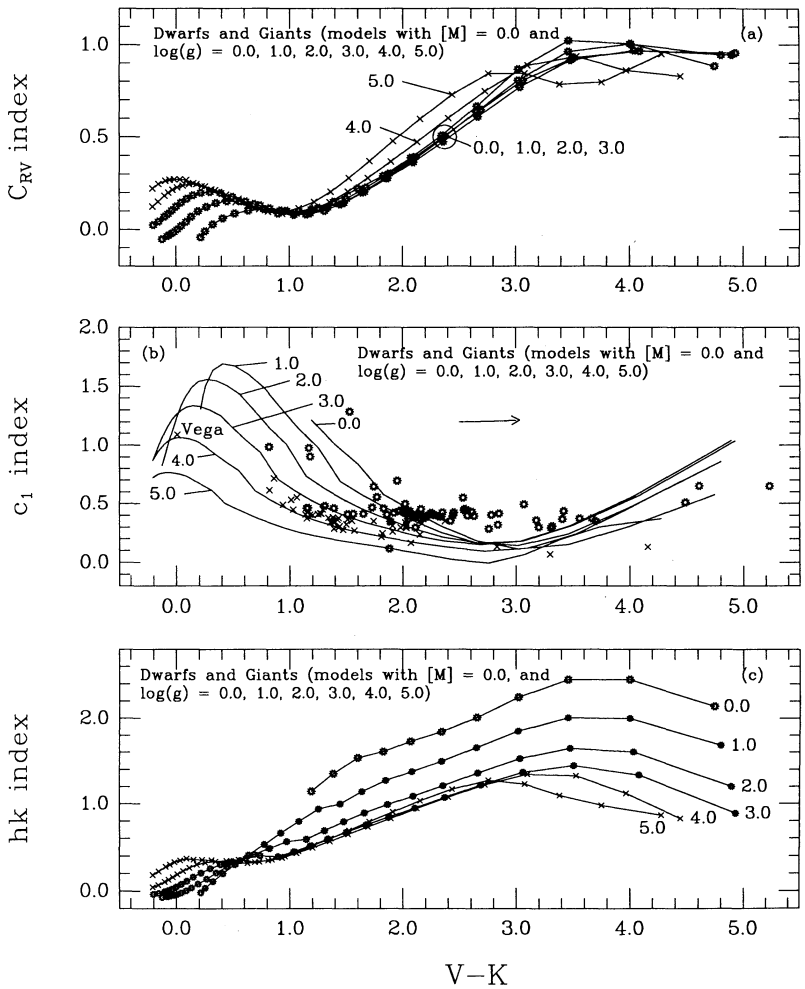

FIG. 10.—(*a*) C_{RV} vs. $V-K$ grids are computed from atmosphere models with [M] = 0.0 and log g = 0.0, 1.0, 2.0, 3.0 (*grid points with open symbols*) and log g = 4.0, 5.0 (*grid points with crosses*) to study the dependence of C_{RV} on log g. (*b*) The c_1 vs. $V-K$ indices observed for a subset of the sample of dwarfs (*crosses*) and giants (*open symbols*) from the HK Project (see Figs. 6*a* and 6*b*, respectively). The arrow in (*b*) indicates the effect of interstellar reddening assuming $E(V-K) = 0.50$ and

$$\frac{E(c_1)}{E(V-K)} = \left[\frac{E(c_1)}{E(b-y)}\right]\left[\frac{E(b-y)}{E(B-V)}\right]\left[\frac{E(B-V)}{E(V-K)}\right] \approx (0.09)(0.7)\left(\frac{1}{2.78}\right) \approx 0.23.$$

The grids are computed from atmosphere models with log g = 0.0, 1.0, 2.0, 3.0, 4.0, 5.0 and [M] = 0.0. (*c*) The *hk* vs. $V-K$ grids computed from atmosphere models with [M] = 0.0 and log g = 0.0, 1.0, 2.0, 3.0 (*grid points with open symbols*) and log g = 4.0, 5.0 (*grid points with crosses*).

giants than for dwarfs). This is probably caused by the departure of the models from LTE for stars of low surface gravity. For all indices, except for the *hk* index where our calibration for the metal-poor grid is unconfirmed, the differences do not seem to depend on [Fe/H].

In summary, the differences for the $b-y$ and m_1 indices are all within ± 0.1 dex for both the dwarfs and the giants on our list. The difference of the c_1 index is significantly larger with a range of ± 0.2 dex. The difference for the C_{RV} index is also within ± 0.15 dex, except for some of the cooler dwarfs and giants. The computed *hk* index agrees to within 0.2 dex with ATLPT observations. We caution that the uncertainties of the derived atmospheric parameters ($\Theta_{\rm eff}$, log g, and [Fe/H]) are mostly unknown, and it remains difficult to make any firm quantitative conclusion on the reliability of the models.

7. SUMMARY

Compared with the photometric indices m_1, c_1, and *hk*, the narrower Mount Wilson C_{RV} index has both advantages and disadvantages. Of the three metallicity indices compared, the *hk* index is the most metal-sensitive index at most values of $b-y$ (or $V-K$) and values of the scaled metal abundance in the range $-1.0 \leq$ [M] ≤ 0.5. However, the calibration of the measured *hk* index to the grid at metal-poor conditions remains unconfirmed.

Although a narrow-band photometric index may not collect enough photons on faint stars to allow for satisfactory statistical errors, it allows specific elements to be calibrated. The C_{RV} index seems to be directly associated with Fe, and it is free from the confounding effects of enhanced α-process elements

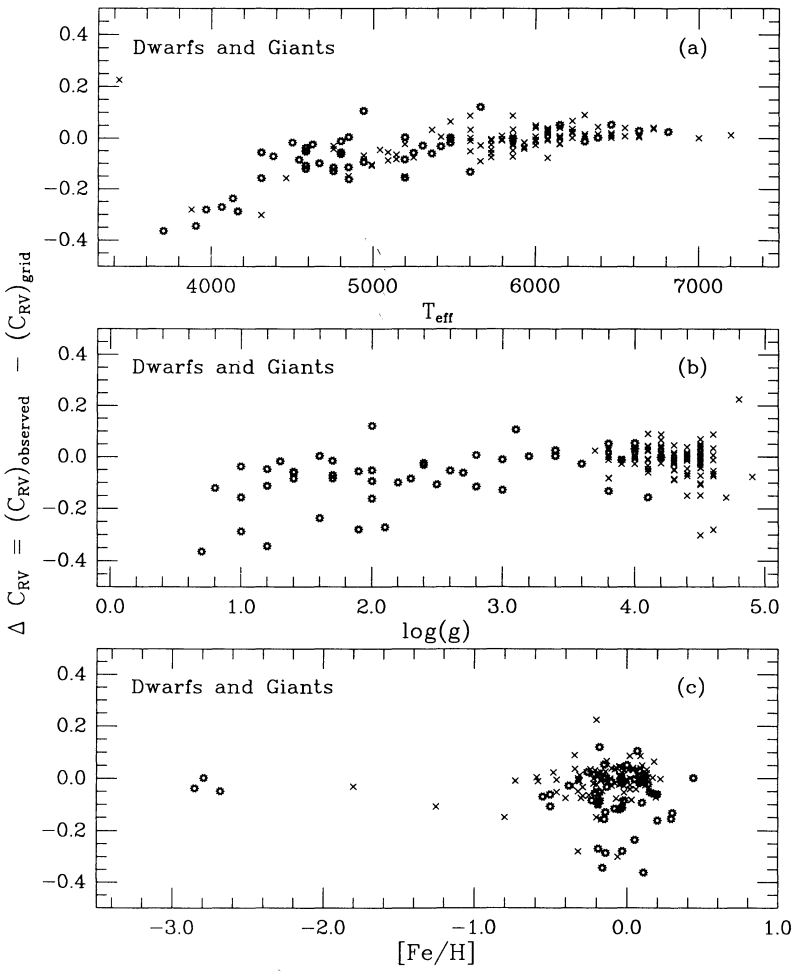

FIG. 11

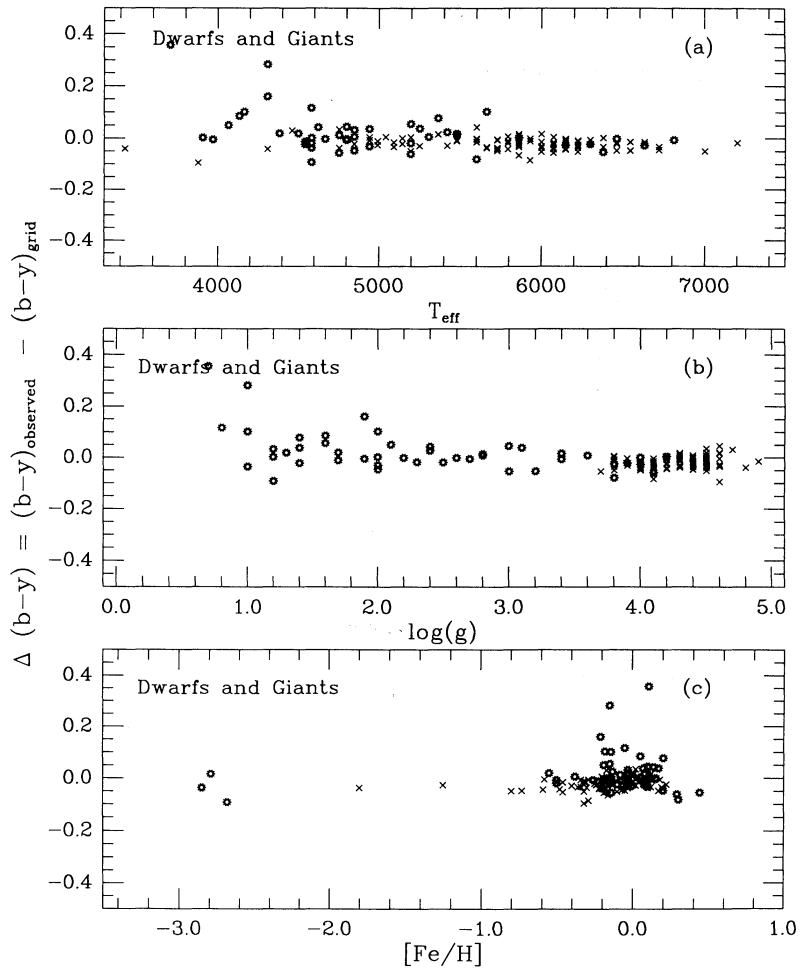

FIG. 12

FIG. 11.—Difference, ΔC_{RV}, between the observed and computed C_{RV} indices as a function of (*a*) T_{eff}, (*b*) log *g* and (*c*) [Fe/H] for the sample of dwarfs (*crosses*) and giants (*open symbols*) from the HK Project which have observed stellar atmosphere parameters.

FIG. 12.—Difference, $\Delta(b-y)$, between the observed and computed $b-y$ indices as a function of (*a*) T_{eff}, (*b*) log *g*, and (*c*) [Fe/H] for the sample of dwarfs (*crosses*) and giants (*open symbols*) studied by the HK Project which have observed stellar atmosphere parameters.

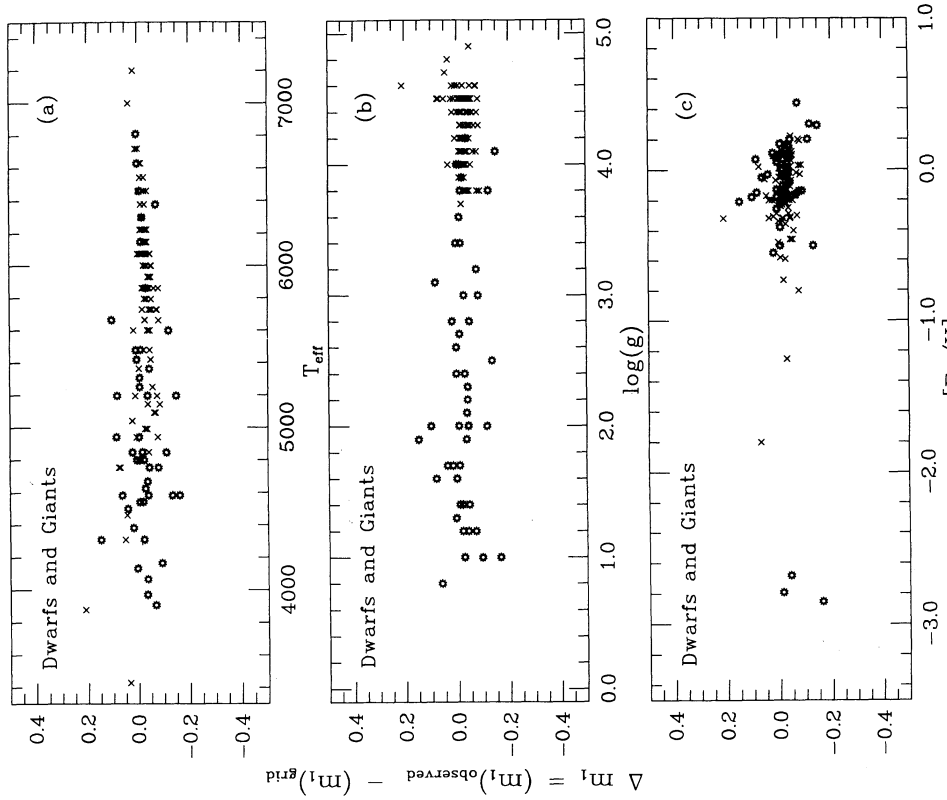

FIG. 13.—Difference, Δm_1, between the observed and computed m_1 indices as a function of (*a*) T_{eff}, (*b*) log *g*, and (*c*) [Fe/H] for the sample of dwarfs (*crosses*) and giants (*open symbols*) studied by the HK Project which have observed stellar atmosphere parameters. Note that the reddest giant on our list HD 36389 (M2 I) has $\Delta m_1 = -0.552$ and is beyond the range of the plot.

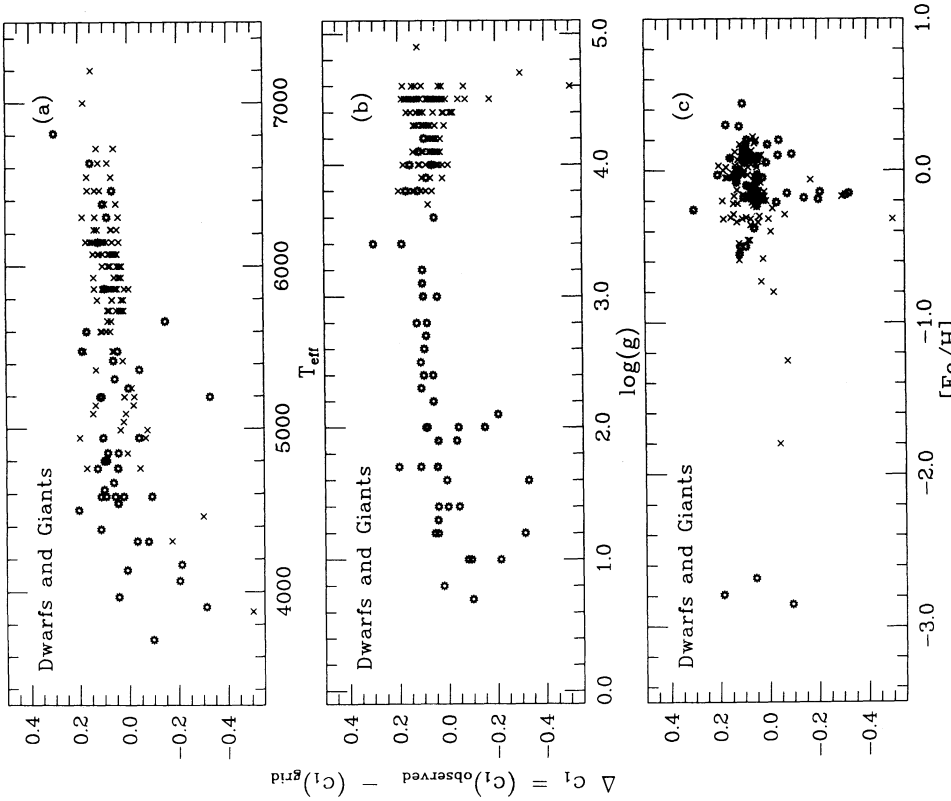

FIG. 14.—Difference, Δc_1, between the observed and computed c_1 indices as a function of (*a*) T_{eff}, (*b*) log *g*, and (*c*) [Fe/H] for the sample of dwarfs (*crosses*) and giants (*open symbols*) studied by the HK Project which have observed stellar atmosphere parameters. Note that the reddest dwarf on our list HD 95735 (M2.5 Ve) has $\Delta c_1 = -0.649$ and is beyond the range of the plot.

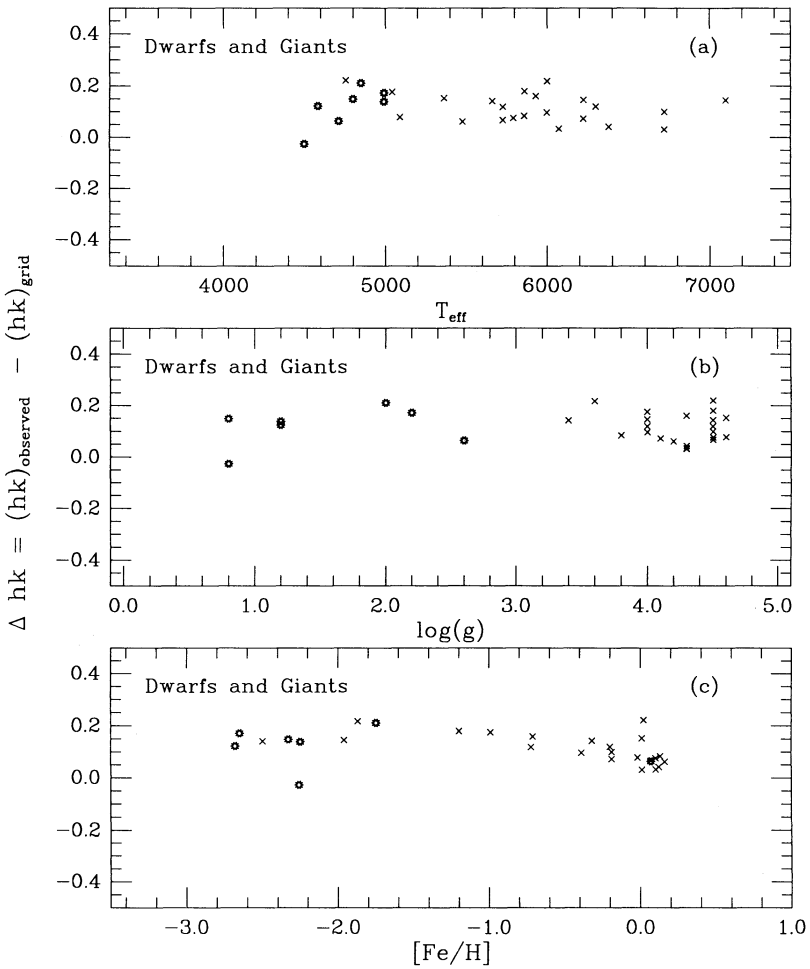

FIG. 15.—Difference, Δhk, between the observed and computed hk indices as a function of (*a*) $T_{\rm eff}$, (*b*) log g, and (*c*) [Fe/H] for the sample of dwarfs (*crosses*) and giants (*open symbols*) from Table 4 of Anthony-Twarog et al. (1991) for which observed stellar atmosphere parameters are available.

under metal-poor conditions. The prospect of calibrating C_{RV} to Fe (hence metal) abundance is good over the range $-5.0 \lesssim [M] \lesssim 0.5$. Hence, the goal of examining the metallicity-age relation for the large sample of lower–main-sequence stars in the Mount Wilson Observatory HK Project also seems promising.

We thank A. Sandage and the referee for valuable discussions. We greatly appreciate the dedicated efforts of our colleagues at Mount Wilson Observatory: M. Bradford, R. Donahue, L. Eklund, J. Frazer, L. Rao, C. Shelton, and A. Vaughan. This work was supported by the Mobil Foundation, the Electric Power Research Institute, the American Petroleum Institute, the Lounsbery Foundation, Space Telescope Science Institute and the Scholarly Studies Program, and the Langley-Abbot and James Arthur funds of the Smithsonian Institution. This research was made possible by a collaborative agreement between the Carnegie Institution of Washington and Mount Wilson Institute.

REFERENCES

Adelman, S. J., & Gulliver, A. F. 1990, ApJ, 348, 712
Anders, E., & Grevesse, N. 1989, Geochim. Cosmochim. Acta, 53, 197
Anthony-Twarog, B. J., Laird, J. B., Payne, D., & Twarog, B. A. 1991, AJ, 101, 1902 (ATLPT)
Baliunas, S. L. 1991, in The Sun in Time, ed. C. P. Sonett, M. S. Giampapa, & M. S. Matthews (Tucson: Univ. Arizona), 809
Baliunas, S. L., & Vaughan, A. H. 1985, ARA&A, 23, 379
Baliunas, S. L., et al. 1993, in preparation
Batten, A. H., Fletcher, J. M., & MacCarthy, D. G. 1989, Eighth Catalogue of the Orbital Elements of Spectroscopic Binary Systems (Victoria: DAO)
Beers, T. C., Preston, G. W., Shectman, S. A., & Kage, J. A. 1990, AJ, 100, 849
Bond, H. E. 1980, ApJS, 44, 517
Cayrel de Strobel, G., Hauck, B., François, P., Thevenin, F., Friel, E., Mermilliod, M., & Borde, S. 1992, A&AS, 95, 273
Cohen, J. G., Frogel, J. A., & Persson, S. E. 1978, ApJ, 222, 165
Duncan, D. K., et al. 1991, ApJS, 76, 383
Eggen, O. J., Lynden-Bell, D., & Sandage, A. R. 1962, ApJ, 136, 748
Gilmore, G., Wyse, R. F. G., & Kuijken, K. 1989, ARA&A, 27, 555
Hardie, R. H. 1962, in Astronomical Techniques, ed. G. P. Kuiper & B. M. Middlehurst (Chicago: Univ. Chicago Press), 178
Hoffleit, D. 1964, Catalogue of Bright Stars (New Haven: Yale Univ. Obs.)
Humphreys, R. M., Kudritzki, R. P., & Groth, H. G. 1991, A&A, 245, 593
Kurucz, R. L. 1991, in Precision Photometry: Astrophysics of the Galaxy, ed. A. G. D. Philip, A. R. Upgren, & K. A. Janes (Schenectady: Davis), 27
Mathis, J. S. 1990, ARA&A, 28, 37
Noyes, R. W., Hartmann, L. W., Baliunas, S. L., Duncan, D. K., & Vaughan, A. H. 1984, ApJ, 279, 763
Peterson, R. C., & Carney, B. W. 1989, ApJ, 347, 266
Relyea, L. J., & Kurucz, R. L. 1978, ApJS, 37, 45
Sandage, A. R. 1986, ARA&A, 24, 421
Soderblom, D. R., Duncan, D. K., & Johnson, D. R. 1991, ApJ, 375, 722
Twarog, B. A., & Anthony-Twarog, B. J. 1991, AJ, 101, 237
Vaughan, A. H., Preston, G. W., & Wilson, O. C. 1978, PASP, 90, 267
Wheeler, J. C., Sneden, C., & Truran, J. W. 1989, ARA&A, 27, 279
Whitford, A. E. 1958, AJ, 63, 201
Wilson, O. C. 1978, ApJ, 226, 379